

This is an Open Access document downloaded from ORCA, Cardiff University's institutional repository:<https://orca.cardiff.ac.uk/id/eprint/158452/>

This is the author's version of a work that was submitted to / accepted for publication.

Citation for final published version:

Monnot, Gwennaëlle C., Wegrecki, Marcin, Cheng, Tan-Yun, Chen, Yi-Ling, Sallee, Brigitte N., Chakravarthy, Reka, Karantza, Ioanna Maria, Tin, Shin Yi, Khaleel, Alexandra E., Monga, Isha, Uwakwe, Laura N., Tillman, Alice, Cheng, Bin, Youssef, Soundos, Ng, Soo Weei, Shahine, Adam, Garcia-Vilas, Javier A., Uhlemann, Anne-Catrin, Bordone, Lindsey A., Han, Arnold, Rohde, Christine H., Ogg, Graham, Moody, D. Branch, Rossjohn, Jamie and de Jong, Annemieke 2023. Staphylococcal phosphatidylglycerol antigens activate human T cells via CD1a. *Nature Immunology* 24 (1) , pp. 110-122. 10.1038/s41590-022-01375-z

Publishers page: <http://dx.doi.org/10.1038/s41590-022-01375-z>

Please note:

Changes made as a result of publishing processes such as copy-editing, formatting and page numbers may not be reflected in this version. For the definitive version of this publication, please refer to the published source. You are advised to consult the publisher's version if you wish to cite this paper.

This version is being made available in accordance with publisher policies. See <http://orca.cf.ac.uk/policies.html> for usage policies. Copyright and moral rights for publications made available in ORCA are retained by the copyright holders.



7 **Staphylococcal phosphatidylglycerol antigens activate human T cells via CD1a**

8 Gwennaëlle C. Monnot¹, Marcin Wegrecki², Tan-Yun Cheng³, Yi-Ling Chen⁴, Brigitte N. Sallee¹, Reka Chakravarthy¹, Ioanna Maria
9 Karantza¹, Shin Yi Tin², Alexandra E. Khaleel¹, Isha Monga¹, Laura N. Uwakwe¹, Alice Tillman^{5,6}, Bin Cheng⁷, Soundos Youssef¹,
10 Soo Weei Ng⁴, Adam Shahine², Javier A. Garcia-Vilas⁵ Anne-Catrin Uhlemann^{5,6}, Lindsey A. Bordone¹, Arnold Han⁵, Christine H.
11 Rohde⁸, Graham Ogg⁴, D. Branch Moody^{3,10}, Jamie Rossjohn^{2,9,10}, Annemieke de Jong^{1,10*}

12 1. Department of Dermatology, Columbia University Irving Medical Center, New York, NY, USA

13 2. Infection and Immunity Program and Department of Biochemistry and Molecular Biology, Biomedicine Discovery Institute,
14 Monash University, Clayton, Victoria, Australia

15 3. Division of Rheumatology, Inflammation and Immunity, Brigham and Women's Hospital, Harvard Medical School, Boston,
16 Massachusetts, USA

17 4. Medical Research Council Human Immunology Unit, MRC Weatherall Institute of Molecular Medicine, University of Oxford

18 5. Department of Medicine, Columbia University Irving Medical Center, New York, NY, USA

19 6. Microbiome and Pathogen Genomics Core, Department of Medicine, Columbia University Irving Medical Center, New York,
20 NY, USA

21 7. Department of Biostatistics, Columbia University Irving Medical Center, New York, NY, USA

22 8. Department of Surgery, Columbia University Irving Medical Center, New York, NY, USA

23 9. Institute of Infection and Immunity, Cardiff University, School of Medicine, Heath Park, Cardiff, UK

24 10. Equal contributions

- 25 * Correspondence to: Annemieke de Jong, Columbia University Irving Medical Center, College of Physicians and Surgeons,
26 Department of Dermatology, Russ Berrie Medical Science Pavilion, room 303B, New York, NY 10032. ad2952@cumc.columbia.edu

27 **ABSTRACT**

28 Expressed on epidermal Langerhans cells, CD1a presents a range of self-lipid antigens found within the skin. However, the extent to
29 which CD1a presents microbial ligands from bacteria colonizing the skin is unclear. Here, we identified CD1a-dependent T cell
30 responses to phosphatidylglycerol (PG), a ubiquitous bacterial membrane phospholipid, as well as to lysyl phosphatidylglycerol
31 (lysylPG), a modified PG, present in several gram-positive bacteria, and highly abundant in *Staphylococcus aureus*. The crystal
32 structure of the CD1a-PG complex showed that the acyl chains were buried within the A'- and F'-pockets of CD1a, while the
33 phosphoglycerol headgroup remained solvent-exposed in the F'-portal and was available for T cell receptor contact. Using lysylPG and
34 PG-loaded CD1a tetramers, we identified T cells in peripheral blood and in skin that respond to these lipids in a dose dependent
35 manner. Tetramer+ CD4+ T cell lines secreted Th2 cytokines in response to phosphatidylglycerols as well as to co-cultures of CD1a+
36 dendritic cells and *Staphylococcus* bacteria. The expansion in atopic dermatitis (AD) patients of CD4+ CD1a-(lysyl)PG tetramer+ T
37 cells suggest a response to lipids made by bacteria associated with atopic dermatitis, and provide a link supporting involvement of PG-
38 based lipid-activated T cells in AD pathogenesis.

39 INTRODUCTION

40 The lipid antigen presenting molecule CD1a is constitutively expressed at extremely high density on Langerhans cells¹, the resident
41 dendritic cell type in stratified epithelia of the skin, mouth, and genital mucosa². The prominent presence of CD1a specifically localized
42 within human epithelia suggests a possible role for lipid antigen recognition by T cells in barrier immunity and homeostasis. In addition,
43 CD1a-expressing Langerhans cells are in close proximity to the epithelial microbiota, suggesting that CD1a may have routine access
44 to microbial lipids from skin surface resident bacteria and fungi and present these to CD1a-restricted T cells³. Despite these anatomical
45 links between CD1a and microbiota, as well as rapidly growing insights into skin microbiome⁴, these connections have not been
46 addressed experimentally. To date, only one CD1a-presented bacterial lipid antigen has been identified: a lipopeptide known as
47 dideoxymycobactin (DDM) from the lung pathogen, *Mycobacterium tuberculosis*^{5, 6}. Since CD1a is most abundantly expressed on
48 Langerhans cells, which survey the skin microbiome⁷, we wanted to use CD1a tetramers to see whether the human T cell repertoire
49 also contains T cells that recognize lipids present in common skin commensals and pathogens.

50 We focused on phosphatidylglycerols (PG), which are highly abundant phospholipids in the membranes of essentially all
51 bacteria^{8, 9}. Further, PG can be modified to form lysyl-phosphatidylglycerol (lysylPG), which is the product of the lysine addition to PG
52 by the bacterial multi peptide resistance factor (MprF) enzyme, expressed in several gram-positive bacteria^{10, 11}. The addition of a lysine
53 moiety to PG creates a positive charge on the molecule, rendering the bacterial membrane more resistant to cationic anti-microbial
54 peptides^{10, 12}, and lysylPG is therefore considered a virulence factor. The membrane of the important human pathogen and common
55 skin colonizer *Staphylococcus aureus* (*S. aureus*), is comprised mainly of PG, lysyl PG, cardiolipin and diglucosyldiacylglycerol
56 (DGDG), where lysylPG and PG are the major structural lipids^{13, 14}. Depending on the strain, lysylPG can constitute between 20-40%

57 of all phospholipids in the *S. aureus* membrane¹¹. Although abundant in *S. aureus*, lysylPG is not unique to this pathogen and can
58 also be produced by other gram-positive bacteria, including other MprF-expressing *Staphylococcus* species, such as *S. epidermidis*.
59 Given that *Staphylococcus* species make up approximately 25% of bacteria on the skin¹⁵, both PG and lysylPG are major components
60 of the host skin microbiome. Since MprF is not expressed in mammalian cells, lysylPG can be considered a true foreign lipid.
61 Furthermore, in mammalian cells, PG is present only at trace levels and localized to mitochondrial membranes¹⁶, supporting the notion
62 that PG is also primarily a foreign lipid. Therefore, we sought to determine whether lysylPG and unmodified PG can be presented in
63 the context of CD1a and elicit a T cell response.

64 Using lysylPG and PG-loaded CD1a tetramers, we identified a previously undescribed population of human T cells that responds to
65 these phospholipids in a CD1a-dependent manner. The crystal structures of CD1a-PG confirmed that PG-based lipids are *bona fide*
66 CD1a ligands bound in the cleft. Using sorted CD1a-lysylPG and PG tetramer+ T cell populations *ex vivo* and *in vitro*, we gain insight
67 in the gene expression profiles of these T cells, their response to *Staphylococcus* bacteria, and expansion in atopic dermatitis patients.
68 Overall, this study identifies a novel bacterial phospholipid-reactive T cell population that likely represents part of the human T cell
69 response to common gram-positive bacteria and is implicated in inflammatory skin disease.

70 RESULTS

71 PG and lysylPG are CD1a binding ligands

72 To investigate if CD1a-restricted T cells respond to bacteria, we sought proof of principle that CD1a can present known lipids
73 from the skin microbiome. We chose the lipids PG and lysylPG because of their abundance in the membranes of *Staphylococcal*
74 species. We developed and validated fluorescently-labeled CD1a tetramers by first testing with a CD1a-autoreactive T cell line
75 originally isolated from human skin (DermT)^{17, 18}. This T cell line responds to CD1a-transfected K562 cells in a CD1a-dependent manner
76 that does not require exogenous lipid (**Figure 1a**). A recent study demonstrated that CD1a-endo tetramers stained CD1a-autoreactive
77 T cells from human skin¹⁸. We confirmed this observation by staining the DermT cell line with CD1a-mock tetramers, revealing a
78 population of CD4+ tetramer+ T cells. (**Figure 1b**). Using fluorescence-activated cell sorting (FACS), this tetramer+ population was
79 purified from the line and expanded in vitro, resulting in a cell population highly enriched for tetramer positive cells. Prior data showed
80 that small hydrophobic lipids, including free fatty acids, nest inside CD1a and allow a CD1a-autoreactive TCR to interact with CD1a¹⁹.
81²⁰. Consistent with these data, CD1a tetramers treated with a short chain C16:1 fatty acid bound the CD1a-reactive DermT cell
82 population, at a similar mean fluorescence intensity (MFI) as the CD1a-mock (**Figure 1c**).

83 We next treated the CD1a monomer with lysylPG, and subsequently tetramerized the lipid-treated biotinylated monomers.
84 CD1a tetramer staining of the DermT cell line was significantly decreased (MFI from 10,003 to 1,848) when CD1a was treated with
85 lysylPG. The decreased tetramer binding suggests that lysylPG binds to CD1a and reduces the DermT cell TCR interaction with CD1a.
86 PG loading of CD1a tetramers similarly reduced the binding of the tetramer to DermT (**Extended Data Figure 1a**). In contrast to this
87 result, but in line with prior observations¹⁸, phosphatidylcholine (PC) did not affect the CD1a tetramer binding of the CD1a-autoreactive

88 TCR. Together these observations with CD1a-autoreactive T cells suggest that PG and lysylPG bind CD1a and displace permissive
89 self lipids from the antigen binding cleft.

90

91 **Crystal structure confirms binding of PG in the CD1a antigen binding cleft**

92 We solved the crystal structure of CD1a-PG with intermediate chain fatty acyl groups (18:0, 18:1) (**Figure 1d, Table 1, Extended Data**
93 **Figure 1b**). The oleoyl (C18:1) acyl tail at the position sn-2 was anchored deep inside the cleft of CD1a fully occupying the available
94 volume of the hydrophobic A' pocket. The stearyl (C 18:0) chain at the position sn-1 sharply turned 90° around Trp14 at the bottom of
95 the cleft and partially filled the F' pocket (**Figure 1d**). In the CD1a-PG complex, the phosphate remained buried within the neck of the
96 F' pocket, near the edge of the A' roof, establishing electrostatic contacts with Arg73 and Arg76. The remaining part of the polar
97 headgroup occupied the F' portal, the only solvent accessible segment of the binding cleft of CD1a. Due to the modest size of the
98 glycerol moiety only ~3% of the lipid surface area was solvent exposed (. Overall, the crystal structure of the CD1a-PG complex
99 confirmed that PG-based lipids are bona fide CD1a ligands.

100

101 **CD1a tetramers identify a population of antigen-specific human T cells.**

102 We next used the CD1a-lysylPG and CD1-PG tetramers to determine if the peripheral blood T cell repertoire contains T cells
103 that specifically bind these tetramers. CD1a-mock tetramer stained a small percentage of T cells (range 0.03 – 0.093% of all T cells)
104 (**Figure 1e.**), which is consistent with the presence of CD1a-autoreactive T cells in peripheral blood ^{17, 21}. Staining with the lysylPG-

105 treated CD1a tetramer also stained a fraction of the peripheral blood T cells (range 0.046 - 0.14%), which was not significantly larger
106 than the percentage of T cells binding the CD1a-mock tetramers, but showed higher mean fluorescence intensity (MFI), where majority
107 of tetramer+ T cells expressed the CD4 co-receptor (**Figure 1f**, Extended Data **Figure 1c**). PG-treated CD1a tetramers also stained a
108 population of tetramer+ T cells, as detected in PBMC from a second set of 6 donors (range 0.043 – 0.149%, **Figure 1g**). Overall, the
109 detection of human T cells binding lysylPG and PG-treated CD1a tetramers, suggests that, human blood contains CD1a-restricted T
110 cells that recognize bacterial phospholipids as antigens.

111 We sought to confirm if the observed tetramer+ population indeed represented T cells that are activated by CD1a-lysylPG
112 complexes. As a first step, we screened additional blood bank donors (n = 21) for the presence of a detectable (> 0.02% of T cells)
113 tetramer+ population *ex vivo* using lysylPG-treated CD1a tetramers. From the donors with the highest percentage of CD1a tetramer
114 staining T cells (n=14) we sorted the tetramer+ T cells by FACS, which resulted in the successful enrichment and expansion of CD1a-
115 lysylPG staining T cell lines from half of these donors (n = 7, donors 213, 325, 350, 834, 921, 966, 003, **Figure 2a**). The tetramer+ T
116 cell population was enriched by a second round of sorting and expansion, yielding T cell cultures with up to >90% of the T cells binding
117 the lysylPG-treated CD1a tetramers (**Figure2b**). Similar to the *ex vivo* analysis (**Extended Data Figure 1c**), the majority of the enriched
118 and purified tetramer+ T cell populations expressed the CD4 co-receptor. Consequently, we focused on the CD4+ tetramer+ T cell
119 subset for follow up experiments.

120 CD1a tetramer staining of the sorted CD4+ T cell lines and clones revealed a staining pattern opposite to that of the CD1a-
121 autoreactive T cells (**Figure 2c**). The specificity of the CD1a restriction was confirmed by the absence of staining of T cells with lysylPG

122 treated CD1b, CD1c or CD1d tetramers, while the loading of lysylPG on these isoforms was confirmed by isoelectric focusing
123 **(Extended Data Figure 2a, 2b).**

124 To determine if direct functional recognition of lysylPG underlies the binding of lysylPG-treated CD1a tetramers to the T cells,
125 we performed an assay in which recombinant biotinylated CD1a was bound to neutravidin plates and loaded with increasing
126 concentrations of lysylPG. Tetramer+ T cells specifically released cytokine in response to lysylPG treated CD1a, and not to untreated
127 CD1a, nor CD1a treated with a control phospholipid (PC) **(Figure 2d)**. Similarly, in antigen presenting cell based assays, tetramer+ T
128 cells responded to lysylPG when loaded on K562 CD1a cells or on Langerhans cells **(Figure 2e)**, suggesting that lysylPG is efficiently
129 loaded onto and presented by CD1a on an antigen presenting cell line. Overall, CD1a-lysylPG reactive CD4+ T cells can be
130 reproducibly isolated from the peripheral blood of unrelated donors, and therefore represent a bona fide CD1a-restricted T cell subset.

131

132 **Phospholipid specificity of CD1a-lysylPG tetramer+ T cells**

133 To gain more insight in the specificity and potential phospholipid cross-reactivity of the CD1a lysylPG tetramer+ T cells, we
134 developed a set of CD1a tetramers loaded with common phospholipids present in mammalian cells, including phosphatidic acid (PA),
135 phosphatidylcholine (PC), phosphatidylethanolamine (PE), phosphatidylinositol (PI) and phosphatidylserine (PS). We further included
136 CD1a-PG tetramers **(Figure 3a)**, which have the core phosphoglycerol epitope but not the lysyl moiety in lysyl-PG. Using these
137 tetramers, we screened the 921a T cell line (pre 2nd sort), which contained a population of CD1a-lysylPG staining CD4+ T cells. As
138 expected, the line did not stain with CD1a-mock tetramers, nor did it stain with PC, PE or PS loaded tetramers **(Figure 3b)**. CD1a

139 tetramers loaded with PA appeared to show weak binding of all the cells, and was therefore not considered antigen-specific. PI loaded
140 tetramers did appear to stain the subset of CD4+ T cells, however, at a MFI lower than lysylPG. PG loaded tetramers stained the cells
141 at similar MFI as lysylPG loaded tetramers .

142 This pattern of tetramer binding was not unique to this T cell line, since an independently isolated CD1a-lysylPG reactive CD4+
143 T cell clone (2114.1) from a different donor, showed a similar phospholipid recognition hierarchy (**Figure 3c**). Also, a CD4-negative T
144 cell clone (from donor 966) bound both the PG and lysylPG loaded tetramers . The tetramer staining with CD1a-PG also translated
145 into functional reactivity, namely in an assay with recombinant CD1a bound to a plate, the, lysylPG reactive T cell line (921a) responded
146 to both lysylPG as well as PG (**Extended Data Figure 2c**). We obtained the T cell receptor (TCR) sequence of a T cell clone from the
147 921 line and generated a recombinant soluble 921.3 $\alpha\beta$ TCR. Using surface plasmon resonance we confirmed that 921.3 TCR was
148 directly recognizing CD1a loaded with PG-based lipid antigens in vitro manifested by nearly identical binding affinity towards CD1a-
149 lysylPG ($K_D = 23.4 \pm 4 \mu\text{M}$) and CD1a-PG ($K_D = 23.3 \pm 5 \mu\text{M}$) (**Figure 3d**).

150 Altogether our data suggested that the phosphoglycerol headgroup was required for recognition, and the lysine head group
151 present on the added antigen was tolerated but not required. We also considered an alternate explanation, namely that the lysine group
152 is hydrolyzed during loading or storage, yielding PG. To distinguish between the two possibilities, we investigated the stability of lysylPG
153 during and after loading onto CD1a.

154

155 **pH dependent stability of lysylPG**

156 Prior studies have suggested that the lysine modification of PG is relatively stable at acidic pH, whereas at higher pH (pH > 7) the
157 lysine headgroup is sensitive to hydrolysis²². We confirmed this pH dependent stability by high performance liquid chromatography
158 coupled with Quadrupole-Time-of Flight mass spectrometry (HPLC-QToF-MS) (**Extended Data Figure 3a**). The pH dependent stability
159 of free lysylPG suggested that lipid loading of CD1a must be performed at low pH to minimize hydrolysis and ensure the formation of
160 intact lysylPG-CD1a complexes. Indeed, isoelectric focusing (IEF) data showed that loading at pH 8 resulted in a band corresponding
161 to the CD1a-lipid complex shifting towards the -1 charge, similar to CD1a-PG complexes (**Extended Data Figure 3b**). This shift was
162 not observed when the lysylPG was loaded at pH 5.5, suggesting that loading at low pH resulted in intact CD1a-lysylPG complexes.
163 This cleavage reaction was more quantitatively measured by HPLC-MS analysis of lipids eluted from CD1a, showing that the low pH
164 loading has no significant effect on lysylPG/PG ratio, similar to the input lipids, in which lysylPG was >90% intact (**Extended Data**
165 **Figure 3c**).

166 To determine if lysylPG is stable once bound to CD1a, we incubated CD1a protein that was loaded with lysylPG at pH 5.5 and was
167 confirmed to contain high lysylPG/PG ratio, overnight at pH 5.0, pH 7.0, and pH 9.0 and analyzed by IEF (**Extended Data Figure 3d**).
168 There was no shift observed in CD1a-lipid complex, and IEF did not reveal a band at -1 charge, which would correspond to CD1a-PG.
169 This suggested that once bound to CD1a, lysylPG is not readily hydrolyzed to PG, even at neutral or high pH.

170 Dual tetramer staining of T cell lines with CD1a-lysylPG and CD1a-PG tetramers loaded at low pH and each labeled with a
171 different fluorophore, revealed multiple tetramer⁺ populations, each with distinct tetramer binding intensities. Specifically, the T cell line
172 from donor 966 showed that, although the majority of the tetramer⁺ T cells bound both CD1a PG as well as CD1a lysylPG, there were

173 also populations that specifically bound CD1a-lysylPG with no binding to CD1a-PG (**Figure 3e**). In the line from donor 834, three
174 different populations bound both tetramers, albeit at different staining intensities.

175 To determine if the repertoire contains T cells that specifically bind CD1a-PG, but not CD1a-lysylPG tetramers, we sorted and
176 expanded CD1a-PG tetramer⁺ CD4⁺ T cells ex vivo, and performed dual tetramer staining. This approach indeed revealed a large
177 population of T cells that stained with CD1a-PG tetramer only, as well as a small population of T cells binding both tetramers (**Extended**
178 **Data Figure 4**). When staining four PBMC samples directly ex vivo with the dual tetramers, we detected three tetramer⁺ populations
179 in 3 out of 4 donors (**Figure 3f**). Overall this analysis demonstrates that the T cell repertoire contains cross-reactive T cells for whom
180 the lysine group is redundant for recognition, but also T cells for which the lysine modification either impairs or promotes TCR binding.
181 The pH dependent sensitivity of lysylPG to lysine hydrolysis further suggests that CD1a tetramers loaded at neutral pH with lysylPG
182 likely capture a polyclonal mixture of T cells that recognize lysylPG, PG or both. We further refer to these tetramers as CD1a-(lysyl)PG
183 tetramers.

184

185 **Gene expression profiles of CD1a-restricted CD4⁺ T cells**

186 To gain insight into the cytokine and chemokine gene expression profiles of CD1a-restricted T cells specific for phosphatidylglycerols,
187 we performed gene expression analysis of three independently derived CD4⁺ polyclonal CD1a-(lysyl)PG tetramer⁺ T cell lines from
188 donors 921 and 966. We analyzed gene expression profiles in response to anti-CD3/CD28 stimulation by bulk RNA-sequencing (RNA-
189 seq). All three independently derived T cell lines showed a very similar cytokine/chemokine expression profile, with a dominant

190 upregulation of Th2 cytokines IL-13, IL-5, and IL-4 (**Figure 4a**). Cytokine genes associated with other T-helper subsets, such as *IL17*
191 / *IL22* (Th17/Th22), *IL21* (Tfh) and *TGFB/ IL10* (Treg) were not expressed or weakly upregulated, although there was some *IFNG* (Th1)
192 upregulation in response to stimulation.

193 We sought to confirm the transcriptional profile at the protein level by intracellular cytokine staining for IL-13 and IL-4 (**Figure 4b**).
194 Beyond Th2 cytokines, the CD1a-lysylPG reactive T cell lines upregulated *CSF2* (GM-CSF), *CSF1* (M-CSF), *IL3*, *LTA* (lymphotoxin
195 alpha), *TNF* as well as chemokine genes *CCL1*, *CCL3*, and *CCL4*. (**Figure 4a**). The RNA-seq data additionally showed a strong
196 upregulation of *GZMB* (Granzyme B), *FASLG* (Fas Ligand) and expression of *PRF1* (perforin), suggesting, beyond Th2, a potential
197 cytotoxic function for lysylPG-reactive T cells.

198 The expression of genes associated with cytotoxicity together with the observed chemokine profile corresponds to previously
199 described cytotoxic CD4+ T cells^{23,24}. Although cytotoxicity is generally thought to coincide with a Th1 cytokine profile, the combination
200 with Th2 cytokines has also been described²⁵. Also, since these T cell lines contained more than one clone, the Th2 and cytotoxic
201 profile could be associated with different individual clones. Next we sought to confirm whether the observed Th2 cytokine profile is more
202 prominent in CD1a-(lysyl)PG tetramer+ than in tetramer- CD4+ T cells by sorting tetramer+ and tetramer- CD4+ T cells from the same
203 donor ex vivo. After one round of in vitro expansion, cytokine gene upregulation was measured by qPCR. In both donors, tetramer+
204 CD4+ showed relatively lower expression of the Th1 cytokine IFN- γ and higher expression of Th2 cytokines IL-4, IL-5 and IL-13 (**Figure**
205 **4c**). Similar results were obtained in a more stringent experiment, where we analyzed tetramer- and tetramer+ CD4+ T cells sorted
206 from a single T cell line, in which all cells been subjected to identical culture conditions (**Figure 4d**). Again these data suggest that
207 CD1a-(lysyl)PG tetramer+ T cells are more likely to be skewed towards Th2 compared to tetramer- CD4+ T cells.

208

209 **Single cell transcriptional analysis**

210 To better understand the gene expression profiles of individual cells *ex vivo*, we performed single cell RNA-seq using Plate-seq (ref) of
211 CD1a-(lysyl)PG tetramer+ CD4+ T cells isolated directly *ex vivo* from two donors from whom we had previously confirmed the presence
212 of CD1a-(lysyl)PG reactive T cells (donors 325 and 921). Unsupervised Uniform Manifold Approximation and Projection (UMAP)
213 analysis revealed six clusters among the sorted CD4+ T cells (**Figure 5a**). Embedding of the tetramer- and tetramer+ on the UMAP
214 showed that these populations largely overlapped, with the majority of all T cells falling in clusters 0 and 1. However, differences in
215 the distribution of tetramer- and tetramer+ CD4+ T cells were clear among other clusters, in particular clusters 4 and 5, where CD1a-
216 (lysyl)PG tetramer+ T cells were overrepresented (**Figure 5b, 5c**).

217 The 10 most variable genes in each cluster are depicted as scaled log-normalized expression values (**Figure 5d**), providing
218 clues regarding the phenotypes and functions of the cell subsets in the clusters. Cluster 5, which contains primarily tetramer+ T cells,
219 has features of cytotoxic CD4+ T cells with expression of granzyme B (*GZMB*), Perforin (*PRF1*), granulysin (*GNLY*), CD94 (*KLRD1*)
220 as well as *CRTAM* and *NKG7*. In addition, chemokines *CCL3*, *CCL4*, *CCL5*, as well as *XCL1* and *XCL2* were increased in cluster 5
221 (**Figure 5d and 5e and Supplementary Figure 3**). This cluster is similar in gene expression to a population of CD4+ T cells recently
222 identified in single cell RNA-seq experiments as cytotoxic CD4+ T cells or CD4+ TEMRA^{23, 26, 27 28}, as well as more innate T cell
223 populations²⁹. Furthermore, the cytotoxicity and chemokine gene expression profile of cluster 5 largely overlapped with that of the
224 CD1a-(lysyl)PG tetramer+ T cell lines (**Figure 4a**), suggesting that the gene expression profiles of the *in vitro* T cell lines correspond
225 with those of tetramer+ T cells *ex vivo*.

226 Since all our tetramer+ T cell lines tested produced Th2 cytokines (**Supplementary Table 1**), we investigated the expression
227 of Th2 associated genes in the single cell data set. *IL4* was minimally detected in the entire RNA-seq dataset, whereas *IL13* gene
228 expression was primarily detected in cluster 2 (**Supplementary Figure 3**). Interestingly, *GATA3*, which is considered a master
229 transcription factor of Th2 cells^{30, 31}, was differentially expressed in cluster 4, in which CD1a-(lysyl)PG tetramer+ were also
230 overrepresented compared to tetramer-negative T cells (**Figures 5b and 5c**). This increased expression of *GATA3* in CD1a-(lysyl)PG
231 tetramer+ T cells may explain the preferential expression of Th2 cytokines in this cell population.

232 Other genes that were differentially expressed in Cluster 4 included *CTLA4*, *TIGIT*, *IL2RA*, *LRRC32* (GARP), *TNFRSF18* (GITR)
233 and HLA class II genes (**Figure 5d, 5e and Supplementary Figure 3**), suggesting that this cluster contained CD4+ T cells with features
234 of regulatory T cells. There was some detection of *FOXP3* expression in this cluster, though overall there was limited detection of
235 *FOXP3* in the entire dataset. Interestingly, *IKZF2* (Helios), which is a member of the Ikaros transcription factor family expressed in
236 Tregs³², was also differentially expressed in cluster 4. Consistent with known percentages of Tregs in peripheral blood CD4+ T cells,
237 previously measured at 1-5%³³, approximately 3% of tetramer-negative T cells fell within cluster 4, yet almost 15% of the tetramer+
238 CD4+ T cells fell in this Treg like cluster (**Figure 5b**). This outcome suggested an overrepresentation of T cells with Treg markers
239 among these CD1a-restricted T cells. Accordingly, gene expression profiles reveal that CD1a (lysyl)PG tetramer+ CD4+ T cells are
240 not a single homogenous subset but instead are found among distinct CD4+ subsets, including those expressing cytotoxic effector
241 molecules, Treg markers, as well as the Th2 transcription factor *GATA3*.

242

243 **CD1a-dependent activation of tetramer+ T cells by Staphylococcus bacteria**

244 To test natural PG/lysylPG compounds, we set up an assay in which dendritic cells (DC) were incubated with live *S. aureus*
245 (SA1113), the membranes of which are primarily composed of PG, lysylPG, cardiolipin, and diglucosyl-diacylglycerol¹³. Next we
246 confirmed the presence of PG and lysylPG in *S. aureus*, and analyzed the major species of PGs and lysylPGs by negative-mode,
247 reversed-phase HPLC-QToF-MS. (**Figure 6a, b, Extended Data Figure 5, 6, and Supplementary Figure 4**). Overall, PG and lysylPG
248 species present in in vitro cultured *S. aureus* consisted of a broad range of chain lengths, with C15:0 primarily found in the sn-2 position,
249 whereas acyl chains in the sn-1 position ranged from C14:0 to C20:0 (**Supplementary Figure 4**). We also included *S. epidermidis* in
250 our co-cultures and lipid analyses, which was confirmed to contain both PG and lysylPG, most commonly harboring C20:0 in
251 combination with C15:0 in the acyl chains (**Extended Data Figure 6, Supplementary Figure 4**), thereby containing on average
252 somewhat longer acyl chains than *S. aureus*.

253 After incubation with *S. aureus* or *S. epidermidis*, the DC were co-cultured with tetramer-sorted CD1a-(lysyl)PG reactive CD4+
254 T cell lines in media in the presence of antibiotics. Three sorted T cell lines were tested (**Figure 6c, and Supplementary Figure 5**)
255 and all three showed IL-13 release in response to *S. aureus* and *S. epidermidis* treated DCs. *S. aureus* did not appear to have a direct
256 effect on the T cells in the absence of DCs, and anti-CD1a blocked the response to DCs, indicating that CD1a was required for T cell
257 activation. Thus, CD1a-(lysyl)PG tetramer+ T cell lines that respond to (lysyl)PG lipid antigen in the context of CD1a, also respond to
258 antigen-containing bacteria. Since the Elispot data specifically measured IL-13, we broadened the cytokine analysis of the T cell lines
259 in response to *S. aureus* and *S. epidermidis* bacteria to measuring multiple T cell cytokines by multiplex cytokine assay
260 (LEGENDplex™). This experiment revealed that beyond IL-13, other Th2 cytokines IL-5 and IL-4 were produced in response to bacteria
261 (**Extended Data Figure 7**).

262 Next, we aimed to more directly determine the recognition of natural *S. aureus* PGs. We purified the *S. aureus* PG using thin
263 layer chromatography (TLC) followed by reversed-phase HPLC, and quantified the resultant PG lipids (**Extended Data Figure 6**). *S.*
264 *aureus* PG was incubated with CD1a monomers, and tetramers were made in parallel to CD1a tetramers with C18:1 PG. Although the
265 *S. aureus* PG treated CD1a tetramers did bind the T cell lines, the MFI was lower than with pure C18:1 PG CD1a tetramers (**Extended**
266 **Data Figure 8**).

267 Overall, the CD1a-dependent activation of phosphatidylglycerol-specific CD1a-restricted T cells in response to Staphylococcus
268 bacteria, supports the notion that these CD1a-(lysyl)PG tetramer+ T cells functionally respond to common skin pathogens and
269 commensals.

270

271 **CD1a-(lysyl)PG tetramer+ CD4+ T cells in atopic dermatitis patients.**

272 Next, we aimed to determine if CD1a-(lysyl)PG-reactive T cells could be detected in human skin. T cells isolated from discarded skin
273 tissue taken at surgery were screened for the presence of tetramer+ T cells by flow cytometry. This revealed the presence of CD1a-
274 (lysyl)PG tetramer staining T cells among polyclonal skin T cells. Similar to the tetramer+ T cells isolated from peripheral blood, a
275 tetramer-enriched T cell line from the skin released IL-13 in a dose-dependent manner in response to (lysyl)PG loaded onto plate-
276 bound CD1a (**Figure 6d**). Thus, normal skin contains CD1a (lysyl)PG-reactive T cells.

277 Atopic dermatitis (AD) is associated with colonization of the skin with *S. aureus*, and in patients, flares coincide with an increase
278 in *S. aureus* bacterial burden^{34, 35}. In addition, the skin barrier is often impaired in AD, possibly increasing exposure of the epidermal
279 Langerhans cells to bacteria and bacterial products³⁶. Last, Th2 cytokines are thought to underlie much of AD pathogenesis, prompting

280 the question whether CD1a-lysylPG reactive Th2 type CD4 T cells are expanded in individuals with AD. To investigate these questions,
281 we initially performed a small pilot study for which we enrolled AD patients (n=7) and healthy controls (n=10). We obtained peripheral
282 blood samples, as well as 4 mm skin biopsies from lesional and non-lesional skin sites from AD patients, and matched skin sites from
283 healthy controls.

284 We investigated the frequencies of tetramer binding T cells in the lesional and non-lesional skin of AD patients with that of
285 healthy controls. In control skin, the numbers of T cells extracted from a 4 mm punch biopsy were too low to allow for an accurate
286 enumeration of low frequency tetramer+ populations directly ex vivo. Therefore, for both healthy and AD skin T cells, we included an
287 in vitro expansion step prior to analysis. We generated sufficient T cell numbers to analyse the frequency of tetramer+ T cells from 7
288 control, 6 AD non-lesional, and 5 AD lesional skin biopsies. There was a trend for increased frequency of CD1a (lysyl)PG tetramer+
289 CD4+ T cells in both lesional and non-lesional AD skin compared to control skin, although this difference did not reach statistical
290 significance (**Figure 6e**). It is important to note though, that absolute numbers of CD4+ T cells in AD dermis have been quantified to
291 be >5x that of normal dermis^{37, 38}, which suggests that in absolute numbers CD1a-(lysyl)PG reactive CD4+ T cells are increased in AD
292 skin.

293 Next we measured frequencies of CD4+ CD1a-(lysyl)PG tetramer+ T cells in PBMC samples from AD patients and healthy
294 controls. Compared to healthy controls, there was a higher percentage of CD4+ CD1a-(lysyl)PG tetramer+ T cells in peripheral blood
295 of AD patients (**Figure 6e**), suggesting that CD4+ T cells specific for phosphatidylglycerols are expanded in AD. Because this was a
296 small pilot study with a large range in specific T cell frequency (<0.1% - >2%), we initiated a larger study including 16 AD patients and
297 13 healthy controls. Also, for the follow up study, we made CD1a tetramers that were incubated with lipid at low pH to maintain intact

298 lysylPG. Screening of the PBMC samples from patients and controls showed that, whereas there was not a significant difference in
299 frequency of CD1a-PG tetramer+ CD4+ T cells, CD1a-lysylPG tetramer+ CD4+ T cells were slightly higher in AD patients than in
300 controls (**Figure 6f**).

301 This result suggests that CD4+ CD1a-lysylPG specific T cells are expanded in the peripheral blood of AD patients. Together with the
302 presence of CD1a-lysylPG tetramer+ T cells in AD skin, this finding prompts the question whether these T cells reflect a response to
303 increased bacterial exposure in AD, and whether they contribute to Th2 mediated pathology in this inflammatory skin disease.

304 **DISCUSSION**

305 The investigation of lipid antigen specificity, diversity and functions of human CD1a-restricted T cells is important to understand
306 their role in within the human immune system. Here, we have identified bacterially-derived phosphatidylglycerols, lysylPG and PG as
307 bona fide CD1a-presented lipid antigens, recognized by populations of human T cells. Our data show that lipid antigen loaded CD1a
308 tetramers are a powerful tool to identify and quantify these T cells in peripheral blood and skin, and isolate them for transcriptomic
309 analysis directly *ex vivo*.

310 Previously, studies in human and mouse CD1-restricted T cells provided precedent that phosphatidylglycerol-based lipids can
311 function as antigens. Unmodified phosphatidylglycerols were identified as antigens for human CD1b-restricted T cells and for murine
312 CD1d-restricted non-invariant NKT cells^{39, 40, 41, 42, 43}. Also, a recent study using a human CD1b and CD1c-transgenic mouse strain and
313 systemic infection with methicillin resistant *S. aureus* (MRSA) provided evidence that CD1-restricted T cells reduced bacterial burden
314 and responded to *S. aureus* lipid fractions containing cardiolipin, PG and lysylPG⁴⁴. Although our study did not address direct anti-
315 bacterial effects of CD1a-(lysyl)PG specific human T cells, follow up work will address whether CD1-(lysyl)PG-reactive T cells may play
316 a protective role against bacterial infection in humans.

317 In the cell membranes of *Staphylococcus* species, which make up approximately 25% of bacteria on human skin¹⁵, PG and
318 lysylPG are the two most dominant phospholipids^{13, 14}. Therefore, these lipids are ubiquitous in the human skin microbiome, suggesting
319 that all individuals have likely been exposed to PG and lysylPG during their lifetime. The ubiquitous nature of these lipids in the skin
320 microbiome, together with the constitutive expression of CD1a is in line with the fact that CD1a-(lysyl)PG tetramer+ T cells were

321 detected in most donors tested. Possibly, activation of these T cells occurs only when there is a damaged skin barrier, an increased
322 skin bacterial burden, or both.

323 LysylPG is uniquely foreign, since the aminoacylation of phospholipids does not occur in mammalian cells. The requirement of
324 low pH to prevent lysine hydrolysis, suggests that lysylPG is a relatively labile antigen. However, in the slightly acidic early endosomal
325 system (pH 6.0) of Langerhans cells as well as in the stratum corneum, where the pH is on average 5.5, lysylPG is likely to remain
326 intact. Dual tetramer staining with PG and lysylPG loaded CD1a tetramers indicated that lysylPG and PG epitopes can be differentially
327 recognized. Thus, the bacteria-specific lysine modification generates an epitope that can affect the T cell response, and therefore, the
328 relative amounts of PG versus lysylPG encountered may shape the CD1a-dependent T cell repertoire against bacteria. This is further
329 corroborated by the observation that CD1a-lysylPG but not CD1a-PG tetramer+ CD4+ T cells were increased in AD patients compared
330 to controls.

331 The crystal structure of the CD1a-PG complex showed that PG occupies the cleft of CD1a in a manner distinct from the
332 previously solved structures of CD1a carrying blocking antigens^{20, 45, 46}. PG is not, strictly speaking, foreign in its biochemical structure,
333 but it is expressed at much higher levels in bacteria compared to mammalian cells. The abundance of PG in most bacterial membranes
334 predicts that T cells that respond to CD1a-PG complexes will likely broadly respond to bacteria besides *Staphylococcus* species.
335 Beyond bacterial membranes, PG is also present in trace amounts in mammalian cells, in mitochondria¹⁶, functioning as a high turnover
336 intermediate for cardiolipin. In addition, PG is present in human lung surfactant where it represents between 5 and 10% of phospholipids
337 ⁴⁷. The fact that PG is not uniquely a foreign lipid prompts the question of what the precise functions are of CD1a-PG specific T cells
338 in the immune system, and in which situations they respond to endogenous PG.

339 The combined results from the RNA-sequencing of the T cell lines and the *ex vivo* single cell RNA-seq show that among CD1a
340 tetramer+ T cells several subsets exist that differ significantly in their gene expression profiles and their presumed effector functions.
341 This outcome implies that to understand the role of these CD1a-restricted T cells in inflammatory skin disease, it will become important
342 to analyze not only the frequency of these T cells by tetramer staining, but also their cytokine profiles and surface marker expression.
343 Given prior studies of IL-22 predominance among skin homing¹⁷ and skin resident T cells¹⁸ that are autoreactive to CD1a, the Th2
344 phenotypes seen in multiple lines of experiments here is particularly striking and provides a possible link of CD1a to Th2-mediated
345 inflammatory skin disease. Future investigation into proinflammatory versus regulatory populations among the tetramer+ T cells will
346 shed light on their functions in disease.

347 In summary, this study has provided insights in a previously unknown subset of CD1a-restricted T cells that responds to
348 phosphatidylglycerols and *S. aureus* bacteria, and can be detected in the circulation of most individuals tested. Ongoing investigations
349 aim to understand the physiological role of this T cell subset and their contribution to epithelial and anti-bacterial immunity.

350

351 **ACKNOWLEDGEMENTS**

352 We thank the NIH Tetramer Core Facility for CD1 proteins, Peter Sims and Michael Finlayson for their advice regarding the analysis
353 of single cell RNA-sequencing data, Andreas Peschel for providing *S. aureus* strain, Quinten Cremers for assistance with ChemDraw,
354 and Ildiko van Rhijn for critical reading of the manuscript. The work is supported by the NIAMS (R01 AR074037, K01 AR068475, P30
355 AR069632 to A.d.J. and, R01 AR048632 to D.B.M.) and the Wellcome Trust Collaborative Award (to D.B.M., G.O. and J.R.) as well as
356 an Irving Scholarship (to A.d.J.). J.R. is supported by an NHMRC Investigator award. G.O. receives funding from the Medical Research

357 Council UK and NIHR Oxford Biomedical Research Centre. This work was supported by the NCI Cancer Center Support Grant (P30
358 CA013696 and used the Genomics and High Throughput Screening Shared Resource, and by the NCATS (UL1 TR001873), as well
359 as funding to CUIMC flow core facilities through S10RR027050 and S10OD020056. We thank the staff of the MX1 beamline of the
360 Australian Synchrotron, part of Australian Nuclear Science and Technology (ANSTO).

361

362 **AUTHOR CONTRIBUTIONS**

363 G.C.M. and A.D.J. conceived the project. G.C.M., R.C., I.M.K., A.E.K. performed T cell and tetramer assays, G.C.M. and I.M. performed
364 analysis of RNA-seq data and data submission, M.W., S.Y.T. and A.S. performed structural analysis and Surface Plasmon Resonance
365 studies, T-Y.C. performed lipid elutions and quantification by HPLC-MS, and A.H. and J.A.G.V. performed single cell sequencing.
366 B.N.S., L.N.U., S.Y., C.H.R. and L.B. recruited and enrolled study subjects and collected clinical specimens, A.T. and A.C.U. provided
367 cultured *S. aureus* and *S. epidermidis* for lipid analysis. Y.L.C., S.W.N. and G.O. completed the tetramer analyses of second patient
368 cohort. B.C. performed statistical analyses. A.d.J. J.R. and D.B.M. provided oversight for experiments and input for the study. A.d.J.,
369 G.C.M. prepared the manuscript with input from all authors.

370

371 **COMPETING INTERESTS STATEMENT**

372 A.d.J. and D.B.M. provide consulting to Pfizer. G.O. and Y.L.C. have relevant research collaborations with UCB and Janssen and a
373 patent related to CD1a. The remaining authors declare no competing interests.

375 **Table 1.** Data collection and refinement statistics on CD1a-phosphatidylglycerol binary complex structure.

376

		CD1a-PG 18:0 18:1
Data collection statistics		
Temperature (K)		100
Wavelength (Å)		0.954
Resolution Range (Å)		44.9 - 2.0 (2.1 - 2.0)
Space group		P 2 ₁ 2 ₁ 2 ₁
Unit cell		
	a, b, c (Å)	42.2 89.8 105.2
	α, β, γ (°)	90.0, 90.0, 90.0
Total reflections		373755 (27820)
Unique reflections		27852 (1996)
Multiplicity		13.4 (13.9)
Completeness (%)		100 (100)
Mean I/σ ₁		11.9 (1.8)
R _{p.i.m.} ¹ (%)		5.1 (46.3)
Wilson B-factor (Å ²)		28
Refinement statistics		
R _{work} ² (%)		19.3
R _{free} ³ (%)		23.0
Non-hydrogen atoms		3469
	macromolecules	3061
	ligands	101
	solvent	307
Protein residues		378
rmsd bonds (Å)		0.005
rmsd angles (°)		0.82
Ramachandran		
	favored (%)	98.1
	allowed (%)	1.6
	outliers (%)	0.3
Average B-factor (Å ²)		40
	protein	39
	ligand	54
	water	39

377 Statistics for the highest-resolution shell are shown in parentheses.

378 $^1R_{p.i.m} = \sum_{hkl} [1/(N-1)]^{1/2} \sum_i | I_{hkl,i} - \langle I_{hkl} \rangle | / \sum_{hkl} \langle I_{hkl} \rangle$

379 $^2R_{work} = (\sum | |F_o| - |F_c| |) / (\sum |F_o|)$ - for all data except as indicated in footnote 3.

380 ³4% of data was used for the R_{free} calculation

381

382

383

384

385

386

387 **FIGURE LEGENDS**

388

389 **Figure 1. CD1a tetramers identify populations of human T cells.**

390 (a) GM-CSF release measured by ELISA in the supernatant of co-culture of a CD1a-autoreactive T cell line (DermT) with CD1a
391 transfected K562 cells (K562 CD1a) and K562 transfected with empty vector (K562, control). Depicted is the mean \pm SD of triplicate
392 cultures. Results are representative of >3 independent experiments. P-values were based on the paired two-tailed t-test. ** $p < 0.01$, ***
393 $p < 0.001$ (p-values: $p = 0.0008$, $p = 0.002$, $p = 0.003$). (b) Flow cytometric analysis of DermT cell line stained with mock-loaded CD1a
394 tetramer before and after FACS sorting and expansion. Percentage of tetramer+ T cells indicated. (c, upper panel) Histograms of
395 DermT tetramer staining with mock loaded CD1c tetramers (CD1c mock), CD1a mock and C16:1 fatty acid loaded CD1a tetramers.
396 (c, lower panel) Histograms of DermT tetramer staining with CD1a mock and lysylPG-loaded CD1a tetramers. (d, upper panel) Crystal
397 structure of CD1a-PG at 2.0 Å. The position of phosphatidylglycerol (green) in the binding cleft of CD1a (grey) formed by the $\alpha 1$ and
398 $\alpha 2$ helices. A' and F' pockets are filled with the oleyl and stearyl acyl tails, respectively. The side chain of Trp14 at the bottom of the
399 cleft is shown in black. The side chains of Arg73 and Arg76 are shown in black and their electrostatic contacts with PG are depicted
400 as magenta lines. (d, lower panel) Surface representation of the membrane-distal segment of CD1a showing the F' portal (marked with
401 red dashed lines) and the solvent-exposed part of the lipid ligand surface (green). (e) Representative dot plot example of staining of
402 PBMC ex vivo with mock-treated CD1a and lysylPG-treated CD1a tetramers, gated on live CD14-/CD19-/CD3+ T cells according to
403 gating strategy in **Supplementary Figure 1a**. (f, left panel) Percentage of CD1a tetramer+ T cell among total live T cells in 6 healthy
404 donors, and (f, right panel) mean fluorescence intensity (MFI) of the tetramer+ T cells in the tetramer gate. Horizontal bars indicate

405 median values. P-values were based on the Wilcoxon matched-pairs signed rank test, two-sided * $p < 0.05$ (p-value: $p = 0.03$. n.s. = not
406 significant. (g, left panel) Percentage of tetramer+ T cells staining with mock-treated CD1a and PG-treated CD1a tetramers, and (g,
407 right panel) MFI of the T cell in the tetramer gate, in an additional set of 6 donors. Horizontal bars indicate median values. P-values
408 were based on the Wilcoxon matched-pairs signed rank test, two-sided n.s. = not significant.

409

410 **Figure 2. CD1a-lysylPG tetramer+ T cells functionally respond to lysylPG antigen**

411 (a) The frequency of T cells staining with lysylPG-treated CD1a tetramers among live T cells from healthy donors ($n = 7$) is indicated
412 directly ex vivo, after 1st sort and expansion, and after a 2nd sort and expansion. Gating strategy for ex vivo tetramer staining according
413 to **Supplementary Figure 1a**. (b) Two examples of tetramer-based enrichment show tetramer staining prior to the 2nd sort and after
414 sort and expansion, gated on live CD3+ T cells. (c) Histograms of CD1a tetramer staining of sorted CD4+ T cell line (921a) and clones
415 (clones 2114.5 and 350.2): staining with lysylPG treated CD1a tetramers (closed histograms) and mock-treated CD1a tetramers (open
416 histograms). (d) T cell lines 921a and 2114 were incubated with plate bound CD1a loaded with indicated lipids: phosphatidylcholine
417 (PC) and lysylPG. GM-CSF was measured in the supernatant after 24 hrs by ELISA. Assays were set up in duplicate, and depicted is
418 the mean \pm SD per condition. Results are representative of 2 independent experiments. P-values were based on the paired two-tailed
419 t-test, * $p < 0.05$, ** $p < 0.01$, n.s. not significant (p-values assay 921a: $p = 0.048$, $p = 0.17$, $p = 0.050$, $p = 0.049$. P-values assay 2114: $p = 0.16$,
420 $p = 0.008$, $p = 0.011$) (e) CD1a transfected K562 cells incubated with increasing concentrations of lysylPG were co-cultured with T cell
421 clone 966.1.4+ and T cell line 325. GM-CSF and IL-13 were measured in supernatant after 24 hrs by ELISA. Assays were set up in
422 duplicate (clone 966.1.4+) or triplicate (T cell line 325), and depicted is the mean \pm SD per condition. Results are representative of 2

423 independent experiments. P-values were based on the paired two-tailed t-test, * $p < 0.05$, ** $p < 0.01$, n.s. not significant. (P-values assay
424 966.1: $p = 0.69$, $p = 0.069$, $p = 0.064$, $p = 0.009$. P-values 325: $p = 0.12$, $p = 0.42$, $p = 0.045$, $p = 0.078$).

425

426 **Figure 3. Phospholipid reactivity of T cells binding lysylPG-treated CD1a tetramers**

427 **(a)** Phospholipid structures: phosphatidic acid (PA), phosphatidylcholine (PC), phosphatidylethanolamine (PE), phosphatidylinositol
428 (PI), phosphatidylserine (PS), phosphatidylglycerol (PG), and lysylphosphatidylglycerol (lysylPG). **(b)** Flowcytometric analysis of CD1a-
429 lysylPG reactive T cell line (921a) stained with CD1a tetramers loaded with indicated phospholipids. Gated for live cells. Results were
430 representative of >3 independent experiments. **(c)** Overlapping histograms of flowcytometric analysis of CD1a-lysylPG reactive T cell
431 clones (2114.1, 966.1.4-) stained with CD1a tetramers loaded with indicated phospholipids. **(d)** Surface plasmon resonance was used
432 to measure the affinity of the interaction between soluble 921.3 TCR and immobilized untreated CD1a (CD1a-endo, red) and PG
433 (green) or lysylPG (blue)- treated CD1a. Shown binding curves correspond to one experiment with two injections for each concentration
434 of the TCR (from 0 to 150 μM). Equilibrium K_D was calculated from two independent measurements. **(e)** Flowcytometric analysis of T
435 cell lines from donors 834 and 966 co-stained with CD1a-lysylPG PE-labeled tetramers and CD1a-PG APC-labeled tetramers. Cells
436 were gated for live CD4+ T cells, and distinct populations of tetramer+ T cells are indicated. **(f)** Flowcytometric analysis of PBMC
437 stained ex vivo with CD1a-lysylPG PE-labeled tetramers and CD1a-PG APC-labeled tetramers. Cells were gated for live CD14-/CD19-
438 /CD3+/CD4+ T cells according to the gating strategy in **Supplementary Figure 1a**. Percentages of single and double tetramer staining
439 cells are indicated in the quadrants.

440

441 **Figure 4. Cytokine gene expression of CD4+ CD1a-(lysyl)PG tetramer+ T cells**

442 (a) Bulk RNA sequencing analysis of three CD1a-(lysyl)PG reactive T cell lines, unstimulated (-) and stimulated (+) with anti-CD3 /
443 CD28 beads. Heatmap displays cytokine and chemokine expression after Variance Stabilizing Transformation of the count data. (b)
444 Flowcytometric analysis of intracellular IL-4 and IL-13 staining of CD1a-(lysyl)PG reactive T cell lines (921a and 966) after 6 hr
445 stimulation with PMA-ionomycin. (c) PBMC from donors 325 and 773 were FACS sorted ex vivo into CD4+ CD1a-(lysyl)PG tetramer+
446 and CD4+ tetramer- cells (gating strategy according to **Supplementary Figure 1a**). After one round of in vitro expansion, cytokine
447 mRNA upregulation in response to plate-bound anti-CD3 (OKT3) was measured using qPCR. Expression values were normalized to
448 β -actin. Depicted is the mean \pm SD of 2-4 replicate qPCR reactions. P-values were based on the paired two-tailed t-test. * $p < 0.05$,
449 ** $p < 0.01$, *** $p < 0.001$. (P-values donor 325: $p = 0.0005$, $p = 0.0002$, $p = 0.0002$, $p = 0.035$. P-values donor 773: $p = 0.0005$, $p = 0.011$,
450 $p = 0.0006$, $p = 0.0027$) (d) CD1a-(lysyl)PG tetramer+ and tetramer- CD4+ T cells from T cell line 834 were FACS sorted, and cytokine
451 mRNA upregulation in response to plate-bound anti-CD3 (OKT3) was measured using qPCR. Expression values normalized to β -actin.
452 Depicted is the mean \pm SD of 2-4 replicate qPCR reactions. P-values were based on the paired two-tailed t-test. ** $p < 0.01$, *** $p < 0.001$.
453 (P-values donor 834: $p < 0.0001$, $p = 0.0009$, $p < 0.0001$, $p = 0.0027$).

454

455 **Figure 5. Single cell RNA-sequencing of CD1a-(lysyl)PG tetramer+ CD4+ T cells.**

456 (a, top graph) UMAP of single-cell RNA-seq data from CD1a-tetramer+ and tetramer- CD4+ T cells. The colors represent cells in the
457 six clusters defined using top variable genes and unsupervised clustering. (a, bottom graph) The tetramer+ and tetramer- CD4+ T cells

458 subsets embedded in the UMAP. The total number of tetramer- and tetramer+ T cells are indicated. **(b)** Bar graph representing the
459 proportions of tetramer+ and tetramer- T cell subsets in each of the six different clusters, **(c)** within each of the six clusters. The number
460 of cells in each cluster is indicated above the bars in the graphs. P-values were based on the one-sample Z-test for proportion.
461 *indicates observed proportion differs significantly from 50%. **(d)** Heatmap of unsupervised clustering analysis featuring top 10
462 discriminative genes per cluster. Log normalized counts were scaled based on z-score distribution. **(e)** Violin plots depict expression
463 levels of markers per cluster. Selected for discriminative genes in clusters 4 and 5.

464

465 **Figure 6. Response to Staphylococcal bacteria and CD1a-(lysyl)PG tetramer+ T cells in Atopic Dermatitis**

466 **(a)** Mass chromatograms of major species of PGs and lysylPGs from *S. aureus* SA1113 were analyzed by negative-mode, reversed-
467 phase HPLC-QToF-MS. The length and saturation of the combined fatty acyl chains were deduced by the detected *m/z* matching the
468 structural formula. **(b)** CID-MS of the most abundant species in PG (left) and lysylPG (right) showed the diagnostic fragments of
469 phosphoglycerol (*m/z* 152.995) and lysine (*m/z* 145.097) for PG and lysylPG, respectively. **(c)** IL-13 ELISpot of purified CD1a-PG
470 tetramer-sorted T cells from lines 325, 834 and 003, co-cultured with monocyte-derived dendritic cells pre-incubated with media or live
471 *S. aureus* or *S. epidermidis* bacteria. CD1a-restriction was determined by pre-incubating DC and bacteria with anti-CD1a (OKT6).
472 Depicted is the mean \pm SD of triplicate co-cultures. P-values were based on the paired two-tailed t-test. n.s. = not significant, * $p < 0.05$,
473 ** $p < 0.01$, *** $p < 0.001$. (P-values donor 325: $p = 0.036$, $p = 0.0059$, $p = 0.0033$, $p = 0.0014$, 0.0038 . P-values donor 834: $p = 0.017$, $p = 0.023$,
474 $p = 0.0032$, $p = 0.018$, $p = 0.0002$. P-values donor 003: $p = 0.0010$, $p = 0.0028$, $p = 0.0058$, $p = 0.0017$) **(d)** CD1a-(lysyl)PG tetramer sorted skin
475 T cell line (skinT4) stained with mock-treated and lysylPG-treated CD1a tetramers and analyzed by flow cytometry, gate: live cells. IL-

476 13 release measured by ELISA in supernatant of co-cultures of skinT4 with plate bound CD1a loaded with indicated concentrations of
477 lysylPG ($\mu\text{g/ml}$). Depicted is the mean \pm SD of duplicate cultures. P-values were based on the paired two-tailed t-test, * $p < 0.05$, ** $p < 0.01$
478 (P-values: $p = 0.006$, $p = 0.014$, $p = 0.033$). Results are representative of 3 independent experiments. (e, left graph) CD1a-(lysyl)PG
479 tetramer staining of expanded skin T cells (controls $n = 7$, AD non-lesional $n = 6$, AD lesional $n = 5$). e, right graph) CD1a-(lysyl)PG tetramer
480 staining of PBMC (controls $n = 10$, AD $n = 7$). Gating strategy according to **Supplementary Figure 1a**). Plotted are the percentages of
481 CD1a-(lysyl)PG tetramer+ CD4+ T cells among all T cells. Medians are indicated with horizontal bars. P-values were based on the
482 exact Wilcoxon rank sum test, two-sided. * $P < 0.05$, n.s. = not significant. (P-values: $p = 0.11$, $p = 0.22$, $p = 0.027$) (f) In a separate cohort
483 of AD patients and healthy controls % of CD1a tetramer+ CD4+ T cells was measured using indicated tetramers (Gating strategy
484 according to **Supplementary Figure 1b**). Plotted are the percentages of CD1a-tetramer+ CD4+ T cells among all T cells for controls
485 ($n = 13$) and AD patients ($n = 16$). Medians are indicated with horizontal bars. For each tetramer, comparison between AD and controls
486 was performed using the exact Wilcoxon rank sum test, two-sided. * $p < 0.05$, n.s. = not significant ($p = 0.72$, $p = 0.094$, $p = 0.87$, $p = 0.012$).

487 **REFERENCES**

488

- 489 1. Murphy, G.F., Bhan, A.K., Sato, S., Mihm, M.C., Jr. & Harrist, T.J. A new immunologic marker for human Langerhans cells. *The New*
490 *England journal of medicine* **304**, 791-792 (1981).
- 491
- 492 2. de Fraissinette, A., Schmitt, D. & Thivolet, J. Langerhans cells of human mucosa. *The Journal of dermatology* **16**, 255-262 (1989).
- 493
- 494 3. Kubo, A., Nagao, K., Yokouchi, M., Sasaki, H. & Amagai, M. External antigen uptake by Langerhans cells with reorganization of epidermal
495 tight junction barriers. *The Journal of experimental medicine* **206**, 2937-2946 (2009).
- 496
- 497 4. Byrd, A.L., Belkaid, Y. & Segre, J.A. The human skin microbiome. *Nature reviews. Microbiology* **16**, 143-155 (2018).
- 498
- 499 5. Moody, D.B. *et al.* T cell activation by lipopeptide antigens. *Science* **303**, 527-531 (2004).
- 500
- 501 6. Kasmar, A.G. *et al.* Cutting Edge: CD1a tetramers and dextramers identify human lipopeptide-specific T cells ex vivo. *Journal of*
502 *immunology* **191**, 4499-4503 (2013).
- 503
- 504 7. Ouchi, T. *et al.* Langerhans cell antigen capture through tight junctions confers preemptive immunity in experimental staphylococcal
505 scalded skin syndrome. *The Journal of experimental medicine* **208**, 2607-2613 (2011).
- 506
- 507 8. Sohlenkamp, C. & Geiger, O. Bacterial membrane lipids: diversity in structures and pathways. *FEMS microbiology reviews* **40**, 133-159
508 (2016).
- 509
- 510 9. Dugail, I., Kayser, B.D. & Lhomme, M. Specific roles of phosphatidylglycerols in hosts and microbes. *Biochimie* **141**, 47-53 (2017).
- 511
- 512 10. Peschel, A. *et al.* Staphylococcus aureus resistance to human defensins and evasion of neutrophil killing via the novel virulence factor
513 MprF is based on modification of membrane lipids with l-lysine. *The Journal of experimental medicine* **193**, 1067-1076 (2001).

- 514
515 11. Slavetinsky, C., Kuhn, S. & Peschel, A. Bacterial aminoacyl phospholipids - Biosynthesis and role in basic cellular processes and
516 pathogenicity. *Biochim Biophys Acta Mol Cell Biol Lipids* **1862**, 1310-1318 (2017).
- 517
518 12. Ernst, C.M. & Peschel, A. MprF-mediated daptomycin resistance. *International journal of medical microbiology : IJMM* **309**, 359-363
519 (2019).
- 520
521 13. Kuhn, S., Slavetinsky, C.J. & Peschel, A. Synthesis and function of phospholipids in *Staphylococcus aureus*. *International journal of*
522 *medical microbiology : IJMM* **305**, 196-202 (2015).
- 523
524 14. Hines, K.M. *et al.* Lipidomic and Ultrastructural Characterization of the Cell Envelope of *Staphylococcus aureus* Grown in the Presence of
525 Human Serum. *mSphere* **5** (2020).
- 526
527 15. Grice, E.A. *et al.* Topographical and temporal diversity of the human skin microbiome. *Science* **324**, 1190-1192 (2009).
- 528
529 16. Morita, S.Y. & Terada, T. Enzymatic measurement of phosphatidylglycerol and cardiolipin in cultured cells and mitochondria. *Scientific*
530 *reports* **5**, 11737 (2015).
- 531
532 17. de Jong, A. *et al.* CD1a-autoreactive T cells are a normal component of the human alphabeta T cell repertoire. *Nature immunology* **11**,
533 1102-1109 (2010).
- 534
535 18. Cotton, R.N. *et al.* Human skin is colonized by T cells that recognize CD1a independently of lipid. *The Journal of clinical investigation* **131**,
536 e140706 (2021).
- 537
538 19. de Jong, A. *et al.* CD1a-autoreactive T cells recognize natural skin oils that function as headless antigens. *Nature immunology* **15**, 177-185
539 (2014).
- 540
541 20. Birkinshaw, R.W. *et al.* alphabeta T cell antigen receptor recognition of CD1a presenting self lipid ligands. *Nature immunology* **16**, 258-
542 266 (2015).

- 543
544 21. de Lalla, C. *et al.* High-frequency and adaptive-like dynamics of human CD1 self-reactive T cells. *European journal of immunology* **41**, 602-
545 610 (2011).
- 546
547 22. Danner, S., Pabst, G., Lohner, K. & Hickel, A. Structure and thermotropic behavior of the Staphylococcus aureus lipid lysyl-
548 dipalmitoylphosphatidylglycerol. *Biophysical journal* **94**, 2150-2159 (2008).
- 549
550 23. Hashimoto, K. *et al.* Single-cell transcriptomics reveals expansion of cytotoxic CD4 T cells in supercentenarians. *Proceedings of the*
551 *National Academy of Sciences of the United States of America* **116**, 24242-24251 (2019).
- 552
553 24. Takeuchi, A. *et al.* CRTAM determines the CD4+ cytotoxic T lymphocyte lineage. *The Journal of experimental medicine* **213**, 123-138
554 (2016).
- 555
556 25. Takeuchi, A. & Saito, T. CD4 CTL, a Cytotoxic Subset of CD4(+) T Cells, Their Differentiation and Function. *Frontiers in immunology* **8**, 194
557 (2017).
- 558
559 26. Patil, V.S. *et al.* Precursors of human CD4(+) cytotoxic T lymphocytes identified by single-cell transcriptome analysis. *Science immunology*
560 **3** (2018).
- 561
562 27. Szabo, P.A. *et al.* Single-cell transcriptomics of human T cells reveals tissue and activation signatures in health and disease. *Nature*
563 *communications* **10**, 4706 (2019).
- 564
565 28. Cano-Gamez, E. *et al.* Single-cell transcriptomics identifies an effectorness gradient shaping the response of CD4(+) T cells to cytokines.
566 *Nature communications* **11**, 1801 (2020).
- 567
568 29. Gutierrez-Arcelus, M. *et al.* Lymphocyte innateness defined by transcriptional states reflects a balance between proliferation and
569 effector functions. *Nature communications* **10**, 687 (2019).
- 570

- 571 30. Zheng, W. & Flavell, R.A. The transcription factor GATA-3 is necessary and sufficient for Th2 cytokine gene expression in CD4 T cells. *Cell*
572 **89**, 587-596 (1997).
- 573
574 31. Flavell, R.A. *et al.* Molecular basis of T-cell differentiation. *Cold Spring Harbor symposia on quantitative biology* **64**, 563-571 (1999).
- 575
576 32. Thornton, A.M. *et al.* Expression of Helios, an Ikaros transcription factor family member, differentiates thymic-derived from peripherally
577 induced Foxp3+ T regulatory cells. *Journal of immunology* **184**, 3433-3441 (2010).
- 578
579 33. Gregg, R. *et al.* The number of human peripheral blood CD4+ CD25high regulatory T cells increases with age. *Clinical and experimental*
580 *immunology* **140**, 540-546 (2005).
- 581
582 34. Leyden, J.J., Marples, R.R. & Kligman, A.M. Staphylococcus aureus in the lesions of atopic dermatitis. *The British journal of dermatology*
583 **90**, 525-530 (1974).
- 584
585 35. Kong, H.H. *et al.* Temporal shifts in the skin microbiome associated with disease flares and treatment in children with atopic dermatitis.
586 *Genome research* **22**, 850-859 (2012).
- 587
588 36. De Benedetto, A. *et al.* Tight junction defects in patients with atopic dermatitis. *The Journal of allergy and clinical immunology* **127**, 773-
589 786 e771-777 (2011).
- 590
591 37. Bos, J.D. *et al.* Predominance of "memory" T cells (CD4+, CDw29+) over "naive" T cells (CD4+, CD45R+) in both normal and diseased
592 human skin. *Archives of dermatological research* **281**, 24-30 (1989).
- 593
594 38. Guttman-Yassky, E. *et al.* Major differences in inflammatory dendritic cells and their products distinguish atopic dermatitis from
595 psoriasis. *The Journal of allergy and clinical immunology* **119**, 1210-1217 (2007).
- 596
597 39. Van Rhijn, I. *et al.* Human autoreactive T cells recognize CD1b and phospholipids. *Proceedings of the National Academy of Sciences of the*
598 *United States of America* **113**, 380-385 (2016).

- 599
600 40. Shahine, A. *et al.* A molecular basis of human T cell receptor autoreactivity toward self-phospholipids. *Science immunology* **2** (2017).
601
602 41. Shahine, A. *et al.* A T-cell receptor escape channel allows broad T-cell response to CD1b and membrane phospholipids. *Nature*
603 *communications* **10**, 56 (2019).
604
605 42. Wolf, B.J. *et al.* Identification of a Potent Microbial Lipid Antigen for Diverse NKT Cells. *Journal of immunology* **195**, 2540-2551 (2015).
606
607 43. Tatituri, R.V. *et al.* Recognition of microbial and mammalian phospholipid antigens by NKT cells with diverse TCRs. *Proceedings of the*
608 *National Academy of Sciences of the United States of America* **110**, 1827-1832 (2013).
609
610 44. Visvabharathy, L. *et al.* Group 1 CD1-restricted T cells contribute to control of systemic Staphylococcus aureus infection. *PLoS pathogens*
611 **16**, e1008443 (2020).
612
613 45. Zajonc, D.M. *et al.* Molecular mechanism of lipopeptide presentation by CD1a. *Immunity* **22**, 209-219 (2005).
614
615 46. Cotton, R.N. *et al.* CD1a selectively captures endogenous cellular lipids that broadly block T cell response. *The Journal of experimental*
616 *medicine* **218** (2021).
617
618 47. Veldhuizen, R., Nag, K., Orgeig, S. & Possmayer, F. The role of lipids in pulmonary surfactant. *Biochimica et biophysica acta* **1408**, 90-108
619 (1998).
620
621
622

623 **MATERIALS & METHODS**

624

625 **Subject enrolment and sample collection**

626 Skin swabs, 4 mm skin biopsies, and blood samples were collected from AD patients and healthy controls enrolled in our study. This
627 study was approved by the Institutional Review Board at Columbia University under protocol # AAAQ9797, and informed consent was
628 obtained from all participants. For the pilot study depicted in Figure 6e, 10 controls and 7 AD patients were enrolled and provided a
629 blood draw and skin biopsies. The age range of the AD patients was 23-63 years (Average: 38 years. Males 71% Females 29%). The
630 age range of the controls was 22 – 34 (Average 29 years. Males 63% Females 37%). AD patients had a confirmed diagnosis of atopic
631 dermatitis, were not on systemic immunosuppressive or immunomodulatory therapy, and did not use topical steroids for 7 days prior
632 to the biopsy. Participants were reimbursed \$200. A separate cohort of atopic dermatitis patient and healthy volunteer samples were
633 collected under good clinical practice guidance with ethics approval at Oxford University Hospitals NHS dermatology clinic (NRES
634 14/SC/0106). For this study, depicted in Figure 6f, 13 controls and 16 AD patients were enrolled and provided a blood draw. The age
635 range of the AD patients was 23-86 years (Average: 45 years. Males 25% Females 75%). The age range of the controls was 26-77
636 (Average: 51 years. Males: 31% Females 69%). AD patients had a confirmed diagnosis of atopic dermatitis and were not on systemic
637 immunosuppressive or immunomodulatory therapy. Informed consent was obtained from all participants. No participant compensation
638 was provided. In addition, we obtained buffy coats from healthy blood donors through the NY blood center, as well as skin tissue as
639 discarded tissue from plastic surgery procedures.

640

641 **Synthetic Lipids**

642 Certain lipids used in for loading on the CD1 monomers, as well as for functional assays, were purchased from Avanti Polar lipids, Inc.
643 C18:1 lysylPG (#840521), C18:1 PC (#850375), C18:1 PE (#850725), C18:1 PA (#840875), C18:1 PS (#840035), C18:1 PI (#850149),
644 C18:1 PG (#840475).

645

646 **Bacterial lipid extraction**

647 Bacterial pellets were washed in sodium acetate buffer (20 mM, pH 4.5) and flash frozen and stored at -80C until extracted. To extract
648 total lipids, 1 ml of frozen *S. aureus* (SA1113) or *S. epidermidis* (ATCC 12228) pellet was resuspended in 6 ml of methanol and equally
649 distributed to three 15-ml conical glass tubes. Chloroform was added to each tube followed by more methanol to give the
650 chloroform/methanol ratio of 1:2 (v/v). After 1 hr of orbital shaking, extracts were collected after centrifugation. The organic solvent
651 was evaporated under nitrogen onto glass and the dried extracts were redissolved in C/M (1:1) at 1 mg/ml and stored at -20 °C.

652

653 **1D TLC purification for *S. aureus* PG and lysylPG.**

654 Described in Supplementary Notes

655

656 **PBMC isolation and lymphocyte isolation from skin samples.**

657 Peripheral blood mononuclear cells (PBMCs) were isolated using Ficoll-paque (GE lifesciences - 17-5442-02) and following
658 manufacturer's instruction. PBMCs were cryopreserved in FBS supplemented with 10% dimethyl sulfoxide (DMSO) and stored in liquid
659 nitrogen.

660 For the estimation of CD1a-(lysyl)PG tetramer+ T cell frequencies in AD patient and control biopsies, lymphocytes were isolated
661 from 4 mm skin punch biopsies using Whole skin dissociation kit (human, Miltenyi Biotec, 130-101-540) according to the manufacturer's
662 protocol. After skin dissociation, the cells were washed in RPMI 1640 (Thermo Fisher Scientific – 61870127) with 10% FBS, L-
663 glutamine, 2-mercaptoethanol, and Antibiotic-Antimycotic (100X, Gibco), then cryopreserved in FBS 10% DMSO, and stored in liquid
664 nitrogen until T cell expansion and analysis.

665 For the recovery of T cells from discarded skin tissue samples for the isolation of CD1a-(lysyl)PG tetramer+ T cells, we used a
666 culture-based method modified from⁴⁸ . Briefly, after removal of subcutaneous fat tissue full thickness skin was cut into pieces of
667 ~1mm³. Tissue pieces were let to adhere to tissue culture plate (6 well plate), after which complete T cell media was added (RPMI-
668 1640 with L-glutamine, 8% human AB serum, non-essential and essential aminoacids, penicillin-streptomycin, 2-mercaptoethanol,
669 Antibiotic-Antimycotic) supplemented with recombinant IL-2 (100 IU/ml) and IL-15 10 ng/ml. After 7-14 days, lymphocytes start spilling
670 out of the tissue, and were harvested, washed and cryopreserved until analysis.

671

672 **Recombinant CD1a expression and purification**

673 Human CD1a/β2m dimers were expressed in human embryonic kidney (HEK) 293S GnTI- cells and purified as previously described¹⁸.

674 The lipid loading was performed at 20C overnight with C18:1 lysylPG (Avanti 840521) or 18:0-18:1 PG (Avanti 840503) solubilized in

675 0.5%CHAPS/20mM Tris pH 8, 150mM NaCl. Unbound lipid and detergent were separated from the protein by ion exchange
676 chromatography using a MonoQ 10/100 GL column (GE Healthcare). For crystallization the expression tags were removed using
677 thrombin (Sigma-Aldrich) and the protein was de-glycosylated with endoglycosidase H (New England BioLabs). For SPR, the protein
678 was biotinylated using BirA ligase. The stability of lysylPG during lipid loading was assessed by incubating CD1a-endo with 10x molar
679 excess of lysylPG or PG with different buffers (50mM citrate pH 5.5 or 50mM MES pH 5.5 or 20mM Tris pH 8) at 20C overnight. To
680 confirm lysylPG stability once bound to CD1a CD1a-lysylPG was incubated at 20C overnight in 0.1M MMT buffer (MES, DL-Malic acid,
681 Tris) at different pH (5 or 7 or 9). Lipid loading and degradation was assessed by isoelectric focusing where 1 µg of protein was run on
682 a 5-8 PhastGel (Cytiva).

683 **Crystallization, structure determination, and refinement**

684 The protein sample was up-concentrated to 2mg/ml and crystallized at 20°C in 20 to 25% polyethylene glycol 1500, 10% DL-Malic
685 acid, MES monohydrate, Tris (MMT) buffer (pH 5 to 6) using previously obtained CD1a-lipid seeds⁴⁶. The crystals were flash-frozen in
686 liquid nitrogen and diffracted at the MX1 beamline (Australian Synchrotron). Data processing and scaling was performed in XDS and
687 Aimless, respectively^{49, 50}. Previously solved CD1a binary structure was used as a search model for molecular replacement phasing in
688 PHASER⁵¹. Upon rigid body refinement in phenix.refine the unbiased electron in the cleft of CD1a was used to build the ligand. The
689 model fit was improved using phenix.refine and performing manual refinement in the program COOT^{52, 53}. The final refinement round
690 led to the R/R-free factors of 19/23% for CD1a-PG complex structure. The quality of the data was confirmed by the Protein Data Bank
691 (PDB) validation server and the final model and structure factor files were deposited in the PDB under PDB ID: 7SH4.

692

693 **Expression, refolding, and purification of recombinant TCRs**

694 The 921.3 and BK6 TCRs were produced using a previously described method²⁰. Briefly, individual α and β chains of the TCR, with an
695 engineered disulfide bond between the TCR α and TCR β constant domains were expressed in BL21 Escherichia coli cells as inclusion
696 bodies and solubilized in buffer containing 8 M urea, 10 mM tris-HCl (pH 8), 0.5 mM Na-EDTA, and 1 mM dithiothreitol. The TCR was
697 then refolded in 5M urea, 50 mM tris-HCl (pH 8), 2 mM Na-EDTA, 400 mM L-Arg-HCl, 0.5 mM oxidized glutathione, and 5 mM reduced
698 glutathione. The refolded solution was dialyzed three times against 10 mM tris-HCl (pH 8.0) for a total of 24h. The dialyzed samples
699 were then purified through DEAE cellulose, hydrophobic interaction chromatography (HIC) and gel filtration chromatography. The
700 quality and purity of the samples were analyzed via SDS–polyacrylamide gel electrophoresis.

701 **Surface plasmon resonance**

702 Soluble monomers of biotinylated CD1a carrying endogenous lipids (CD1a-endo) or loaded with specific lipids (CD1a-lysylIPG or CD1a-
703 PG) were coupled onto a streptavidin chip (Cytiva) to a mass concentration of ~2500 resonance units per flow cell. Increasing
704 concentrations of the 921.3 or BK6 TCRs (0 to 150 μ M) were injected over all flow cells for 60 s at a rate of 5 μ l/min on Biacore T200
705 in 20 mM tris-HCl (pH 8), 150 mM NaCl, 0.5% bovine serum albumin (BSA) buffer. The total binding response was calculated in
706 Scrubber2 after subtracting the non-specific binding to an unrelated protein. The KD was calculated using one-site specific binding
707 model in GraphPad.

708

709 **CD1a Tetramers**

710 Biotinylated CD1a monomers were provided by the NIH tetramer facility. Lipids were solubilized in pre-warmed phosphate-buffered
711 saline (PBS, pH 7.4) containing 0.5% 3-cholamidopropyl dimethylammonio 1-propanesulfonate (CHAPS) in a glass tube, incubated at
712 56°C for 30min and then sonicated at 37°C for 30min to solubilize the lipid. CD1a monomer (molar ratio lipid : CD1a = 50 : 1) was then
713 added to the solution with as well as sodium azide (0.02%). The sample was incubated overnight (16 hrs) at 37°C. The next day, the
714 monomers were tetramerized by adding streptavidin-PE (Thermo Fisher Scientific - s866A SAPE) in 6 x 1.8 µl in 10 minute intervals
715 or adding streptavidin-APC (Thermo Fischer Scientific –s868) in 6 x 1.2 µl in 10 minute intervals to 48µl of CD1a-lipid solution. Final
716 concentration was ~ 0.15 µg/µl of CD1a monomer. To minimize the lysine hydrolysis of lysylPG during loading, we established an
717 alternative protocol, which we used to make CD1a-PG and CD1a-lysylPG tetramers for stainings in Figures 3e, 3f. 6f. Lipids were
718 solubilized in MES buffer (20mM, pH 5.6) containing 0.5% CHAPS and sonicated for 30 minutes at 37°C, then incubated with CD1a
719 monomer (ratio lipid ; CD1a 50 : 1) for 1 hr at 37°C. Excess lipid and detergent were removed using Amicon Ultra-0.5 centrifugal filter
720 unit, 30 kDa by washing of the loaded CD1a monomer with PBS. The monomers were then tetramerized as described above.

721

722 **Tetramer staining and isolation of CD1a tetramer⁺ T cells by FACS**

723 PBMCs were thawed and plated at a density of ~ 1.5 x 10⁶ cells/ml in complete T cell media (Fisher Scientific - 61870127)
724 supplemented with 8% human AB serum (Sigma-Aldrich H4522) and 1 ng/ml IL-15 (Peprotech - 200-15). The following day, cells were
725 washed with staining buffer (PBS 2%FBS), incubated at a concentration of max. 0.5 x 10⁶ cells in 25 µl of buffer, and 1 µl of CD1a
726 tetramer for 30 minutes at 20-25°C. Without washing, 0.1 µg of anti-CD3 monoclonal antibody (OKT3, BioLegend - 317325) was added

727 in a 10 µl volume and the sample was incubated at 37°C for 10 minutes. Finally, fluorescently-labelled surface antibodies were added
728 to the staining mix: CD14 BV421 (Biolegend - 301830), CD19 BV421 (Biolegend 302234), CD3 BB515 (BD 564466), CD4 Pe-cy7
729 (Biolegend 300515) and incubated on ice for 20 minutes. 4',6-Diamidino-2-Phenylindole, Dilactate (DAPI) (Biolegend, 422801) was
730 used to exclude dead cells. A BD Influx analyzer was used for the FACS-sorting of the tetramer positive cells. Flowjo v10 was used to
731 analyze flowcytometry data.

732

733 **Culture and expansion of CD1a-tetramer⁺ T cells**

734 Tetramer⁺ T cells were sorted directly in U-bottom 96-well plates containing 10⁵ PBMC irradiated at 2500 rad, 100 IU/ml IL-2
735 (PeproTech - 200-02), 10ng/ml IL-15 (PeproTech - 200-15), and 30ng/ml OKT-3 (BioLegend - 317325), and incubated in cell culture
736 incubator (37°C, 5% CO₂). Fresh medium (RPMI 8% Human AB serum) supplemented with 20 ng/ml IL-15 was added every 2-3 days.
737 After 10-14 days sorted and expanded T cells were tested for enrichment by CD1a tetramer staining.

738 **Supplementary Table 1** provides an overview of all donors, polyclonal T cell lines, and T cell clones as well as the experiments in
739 which they were used.

740

741 **CD1a plate Assay**

742 Plate-binding assays were performed as previously described¹⁹. Briefly, neutravidin plates (Thermo Fisher Scientific, 15129) were
743 coated for 6 hours at 20-25°C with 2.5µg/ml anti-CD11a (Biorad, MCA1848) and 10µg/ml biotinylated CD1a monomers (NIH). Lipid of
744 interest was sonicated in 37°C PBS 0.05% CHAPS (37°C) in a glass tube and sonicated for 30 minutes at 37°C. After coating, plates

745 were washed 3x with warm PBS. 50µl of lipid solution per well was added for overnight incubation at 37°C. The next day, plates were
746 washed 3x with warm PBS, and 1×10^5 T cells per well were added. Supernatant was collected after 24h for ELISA.

747

748 **CD1a antigen presenting assay using CD1a transfected antigen presenting cells**

749 Lipids of interest were suspended in complete T cell medium (RPMI 1640) supplemented with 10% FBS and sonicated at 37°C for 20
750 minutes. As antigen presenting cells, K562 cells were used, which were stably transfected K562 cells with CD1a¹⁷. Sonicated lipid
751 solution and 5,000 antigen presenting cells (APCs) were combined in a 96-well plate and incubated for 1h at 37°C. T cell lines were
752 added at a 5:1 or 10:1 T cell:APC ratio. Supernatant was collected at 24hr and cytokine was measured in the supernatant by ELISA.

753

754 **Dendritic cell (DC) and *S. aureus* / *S. epidermidis* co-culture assay**

755 CD1a-(lysyl)PG tetramer+ T cell lines were thawed and rested overnight (16hrs) in culture media supplemented with recombinant
756 human IL-15 (1 ng/ml). The following day, the CD4+ tetramer+ T cells were sorted by flow cytometry from the T cell lines and were
757 again incubated overnight with IL-15 (1 ng/ml). *Staphylococcus aureus* (SA113) and *Staphylococcus epidermidis* (ATCC 12228) were
758 grown for 16 hrs in LB broth at 37°C on a shaker. A 96-well filtration plate with 0.45µm hydrophobic high protein binding immobilon-P-
759 membrane from Millipore was prepared for IL-13 ELISpot assay (Mabtech) as per the manufacturer's protocol. Approximately, 6000-
760 8000 DCs in a volume of 50 µl/well were co-cultured in a 96-well U-bottom plate with 50 µl of 10^5 /ml concentration of *S. aureus* or
761 *S. epidermidis* in RPMI 1640 (Thermo Fisher Scientific - 61870127) supplemented with 10% FBS without antibiotics. The cells and

762 bacteria were co-cultured in the cell incubator at 37°C for 30 minutes. Final concentration of 100 µg/ml gentamicin in complete RPMI
763 1640 media 10% FBS was added to all the wells. Anti-CD1a blocking antibody (clone OKT6) was added at a final concentration of 20
764 µg/ml to the lanes that required the CD1a blocking antibody. The plate was then incubated at 37°C for 60 minutes. After incubation,
765 the cells were transferred from the 96-well U-bottom plate to the coated and blocked IL-13 ELISpot plate and approximately 15,000 T
766 cells in a volume of 50 µl/well were then added to the wells. The Elispot plate was incubated for 24 h at 37°C after which the supernatant
767 was harvested for multiplex cytokine analysis and the IL-13 ELISpot assay (Mabtech) completed according manufacturer's protocol.
768 Cytokine analysis in the supernatant was performed using LEGENDplex™ human T helper cytokine panel (Biolegend 741027)
769 according to manufacturer's protocol.

770

771 **Intracellular cytokine staining (ICS)**

772 Tetramer+ T cell lines were stimulated with PMA-ionomycin (Cell Stimulation Cocktail, eBioscience 00-4970-03), in cell culture
773 incubator. After 30 minute Golgistop (monensin) was added and cells were incubated for an additional 4 hrs and 30 minutes. Cell were
774 stained with fixable live/dead marker (Thermo Fisher Scientific, L23105), and then fixed and permeabilized using Fix/Perm buffer and
775 further processed and stained according to the protocol for intracellular cytokine staining using Fixation and Permeabilization Solution
776 Kit with BD GolgiStop™ (Cat. No. 554715). Antibodies used for ICS and surface stains: CD4-PE (Biolegend, 300508), CD3 APC
777 (Biolegend, 300412), IL-4 Alexa fluor 488 (Biolegend, 500817), IL-13 V450 (BD Bioscience, 561158).

778

779 **LysylPG stability test and HPLC-MS analysis**

780 For lysylPG stability test at different pH values, 10 µg of lysylPG was incubated in the tetramer loading buffer at pH 5.6, 7.4 or 8.0
781 either at 20-25°C (RT) overnight (o/n) or 37 °C for 1 hour. For lysylPG recovery from lipid-loaded CD1a proteins purified CD1a was
782 incubated at 20°C overnight with 15X molar excess of lysylPG or PG dissolved in 0.5% CHAPS, 150mM NaCl and either 50mM MES
783 pH 5.5 or 20mM Tris pH 8. The protein was separated from the excess lipid and detergent by size exclusion chromatography run in
784 150mM NaCl and either 50mM MES pH 5.5 or 20mM Tris pH8. 50 µg samples of lipid loaded CD1a were used for mass spectrometry
785 analyses. These samples were extracted by chloroform, methanol, and water ⁵⁴. The organic phase from each sample was collected
786 and dried under nitrogen gas. Before the injection for HPLC-MS analysis, the lipid extract from the tetramer buffer was normalize to
787 2.5 µM in the starting mobile phase, whereas the eluent residue from the CD1a protein was normalized to 25 µM based on the protein
788 concentration. These samples were run on an Agilent Poroshell 120 A, EC-C18, 3 x 50 mm, 1.9 µm reverse phase column coupled
789 with a 3 x 5 mm, 2.7 µm reverse phase guard column and analyzed by an Agilent 6546 Accurate-Mass Q-ToF/1260 series HPLC
790 instrument. The binary solvent systems were used as described ⁵⁵. For PG and lysylPG quantification, a series of concentrations of
791 these two synthetic standards were prepared. The chromatogram areas from the HPLC-MS analysis were plotted against the
792 corresponding concentrations to generate the standard curves. The unknown lipid concentrations of lysylPG or PG were estimated by
793 external standard curve fitting (**Extended Data Figure 3**).

794

795 **Fatty acid methyl ester (FAME) preparation and HPLC-MS analysis.**

796 Described in Supplementary Notes.

797

798 **Nanoelectrospray CID-MS analysis of PGs.** 50 µg of the total lipids from *S. aureus* or *S. epidermidis* were dissolved in 100 µl of
799 methanol. 10 µl of the methanol solution was loaded onto a nanospray tip for negative-mode ESI-MS and CID-MS using LXQ Linear
800 Ion Trap Mass Spectrometer (Thermo Scientific). The spray voltage was set to 0.7 kV and the capillary temperature was set at 200 °C.
801 For the CID-MS, collision energy was 20–30% of maximum and product ions were trapped with a q value of 0.25.

802

803 **Single cell RNA-sequencing using PLATE-seq (pooled library amplification for transcriptome expression sequencing)⁵⁶**

804 PBMCs were thawed and incubated in cell culture incubator overnight in complete RPMI (Thermo Fisher Scientific - 61870127)
805 supplemented with 8% human AB serum (Sigma-Aldrich H4522) and 1 ng/ml IL-15 (Peprotech - 200-15). The next day, PMA_ionomycin
806 based cell stimulation cocktail (eBioscience 00-4970-03) was added to the cells for 2.5 hours prior to CD1a tetramer staining.. The
807 gating strategy included: lymphocyte gate, gating out of doublets, dead cells, CD14+, CD19+ cells, and positive selection for CD3+
808 CD4+ (**Supplementary Figure 1a**). To avoid confounding plate effects, we designed the plates so that tetramer⁺ and tetramer⁻ T cell
809 subsets were represented on each plate, rather than separate plates per subset⁵⁷. Individual tetramer⁺ and tetramer⁻ CD4⁺ T cells
810 were sorted with a BD Influx analyzer into the wells of a 96-well plate, each containing 7.5 µl of lysis buffer [0.2% Triton X-100 (Sigma),
811 SUPERaseIN (1 U/µl) (Thermo Fisher Scientific), 2 mM deoxyribonucleotides (dNTPs) (Thermo Fisher Scientific), and 2 µM reverse
812 transcriptase (RT) primer (Integrated DNA Technologies)]. Primer annealing was performed at 72°C for 3 min. Reverse transcription
813 was performed by adding 7.5 µl of RT mix to each well [containing: 40U Maxima H- (Thermo Fisher Scientific), 2X Maxima H- Buffer
814 (Thermo Fisher Scientific), 4U SUPERaseIN (Thermo Fisher Scientific), 15% polyethylene glycol, 2µM Template Switching Oligo

815 (Integrated DNA Technologies)]. Further sample processing and library preparation was performed by the Single Cell Analysis Core of
816 Columbia University according to published protocol ⁵⁸, and libraries were sequenced on Illumina NextSeq 500 using the 75-cycle High
817 Output Kit [read lengths 26(R1) × 8(i) × 58(R2)]. Custom sequencing primers were used for Read 1 (SMART_R1seq and ILMN_R1seq;
818 ⁵⁶). With each plate, ~70 million reads were targeted. Library pools were loaded at 1.8 pM with 30% PhiX (Illumina).

819 **Analysis of single cell RNA-seq data**

820 Reads were aligned to the human genome reference GRCh38 using STAR (version 2.5) ⁵⁹. During alignment, reads with more than
821 one mapping were recorded as unmapped using the arguments ‘—out FilterMultimap N max 1’ and ‘—out SAMunmapped Within’ .
822 Alignment counts were generated using featureCounts function of the Subread package (version 1.6)⁶⁰ . Reads were assigned to cell
823 and unique molecular indicator (UMI) barcodes using UMI-tools ⁶¹. The resulting gene-abundance files were analyzed using the Seurat
824 V4 workflow. Briefly, the gene-count matrices were first screened for initial Quality control (QC) checkpoints. In short, genes that were
825 expressed in less than 3 cells were removed from the analysis, as well as cells that had less than 200 genes expressed. Moreover,
826 cells that had a total UMI count of less than 200 or more than 5000 or a percentage of mitochondrial reads higher than 11% were
827 removed from the analysis⁶². After the initial QC and pre-processing to remove the unwanted, dying cells or doublets, RNA counts
828 were log-normalized and then merged using identified anchors (**Supplementary Figure 2**). Further, contaminating APCs forming a
829 separate cluster and overexpressing DCs markers were also removed from the analysis. The dataset from donor 325 included a
830 separately sorted population of CD1a mock staining CD4+ T cells, which was also removed from the analysis. The datasets from two
831 donors were merged using ‘merge’ followed by clusters computation, data scaling and data normalization using the ‘FindClusters’,
832 ‘Normalizeddata’ and ‘ScaleData’ functions respectively. Cluster markers were identified using ‘FindMarkers’ function in Seurat with

833 default parameters for differential expression test. Dimensionality reduction was performed using PCA and UMAP using RunPCA and
834 RunUMAP functions. The heatmaps were generated using DoHeatmap.

835

836 **Bulk RNA-sequencing of CD1a-lysylIPG tetramer+ CD4+ T cells**

837 Described in Supplementary Notes

838

839 **Cell lines used**

840 K562 CD1 stable transfectants were used in antigen presentation assays. The basis for this cell line is the K562, which is not on the
841 list of commonly misidentified cell lines. Although we have not performed genetic testing of this cell line, we routinely check surface
842 expression of HLA class I (absent/low), HLA DR (absent) and CD1 (positive on the transfected cells) by flow cytometry.

843

844 **Statistics**

845 Paired data were compared using the paired t-test with equal or unequal variance, depending on the result of the variance test. Data
846 from independent samples were compared using the exact Wilcoxon rank sum test.

847

848 **Data availability**

849 The CD1a-PG final model and structure factor files were deposited in the Protein Data Base (PDB) under PDB ID: 7SH4.

850 Single-cell and bulk RNA-sequencing files are available in Gene Expression Omnibus (GEO) under accession number GSE186459

851

852 **Code availability**

853 The Seurat object (RDs file format), intermediate output files and differential expression files (csv format) along with the code used in
854 this manuscript for single-cell and bulk RNA-seq analysis is available in GitHub project repository ([https://github.com/IshaMonga/CD1a-](https://github.com/IshaMonga/CD1a-single-cell)
855 single-cell)

856

857

858 **References Methods**

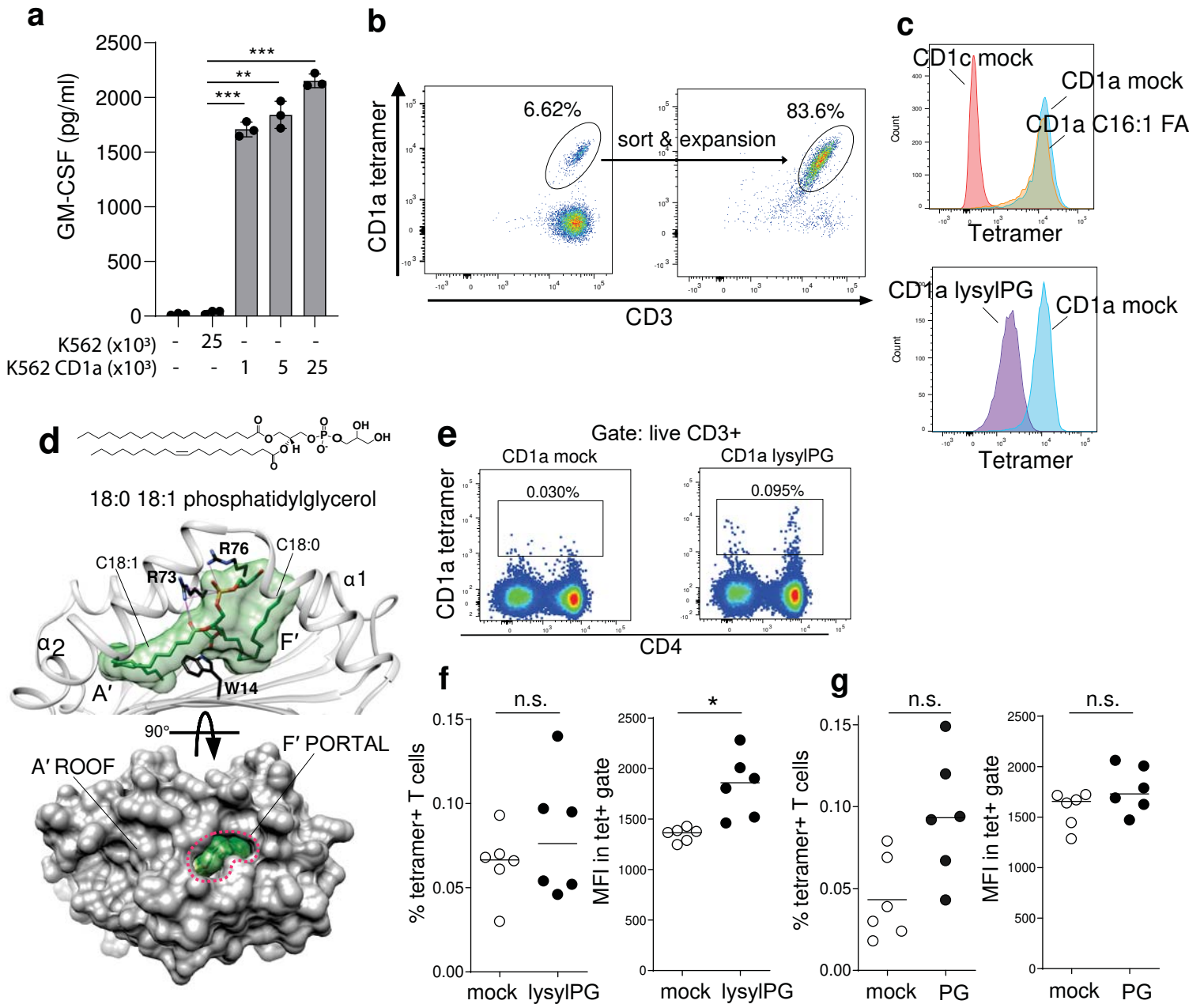
859 48. Clark, R.A. *et al.* A novel method for the isolation of skin resident T cells from normal and diseased human skin. *The Journal of*
860 *investigative dermatology* **126**, 1059-1070 (2006).

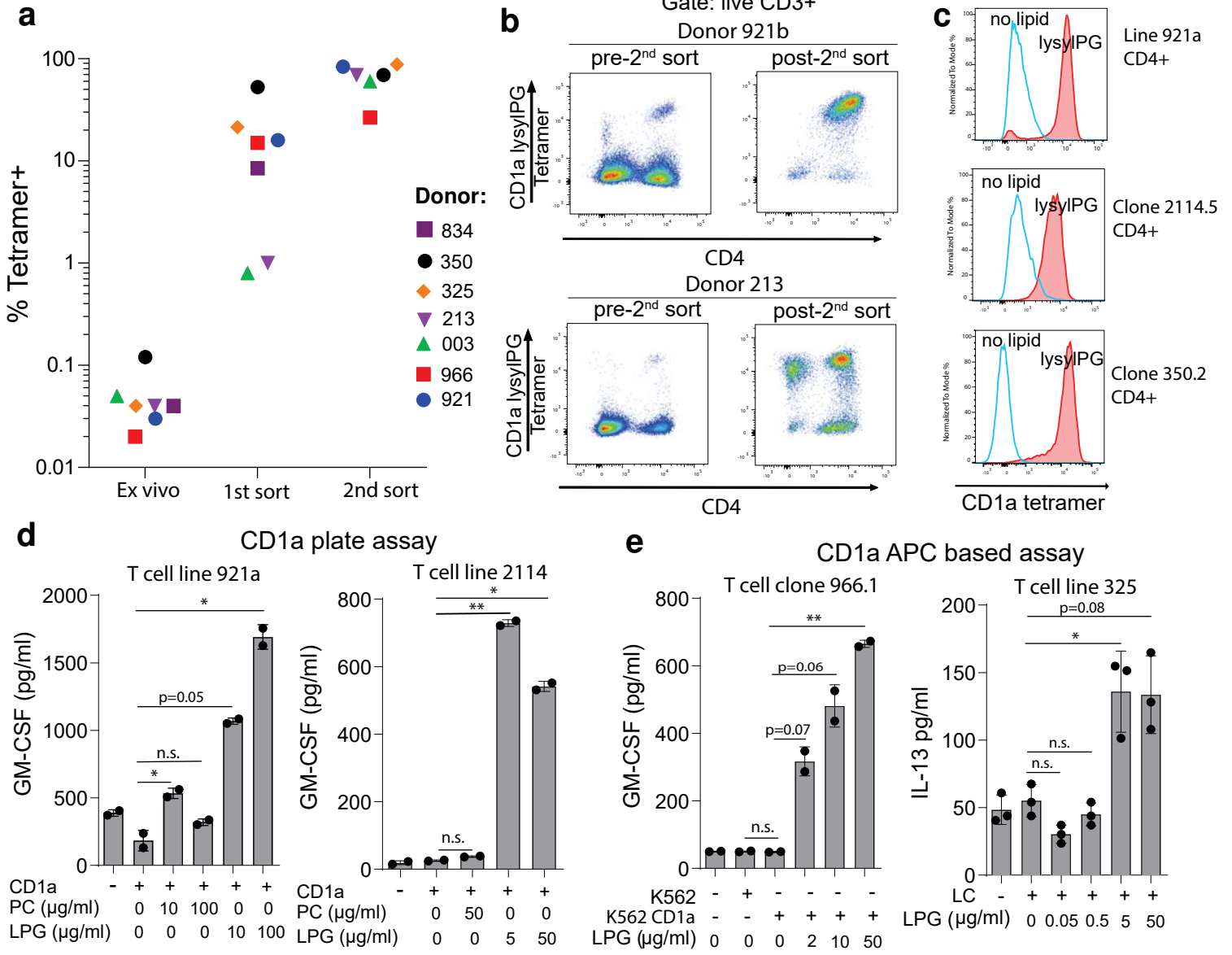
861
862 49. Kabsch, W. Xds. *Acta crystallographica. Section D, Biological crystallography* **66**, 125-132 (2010).

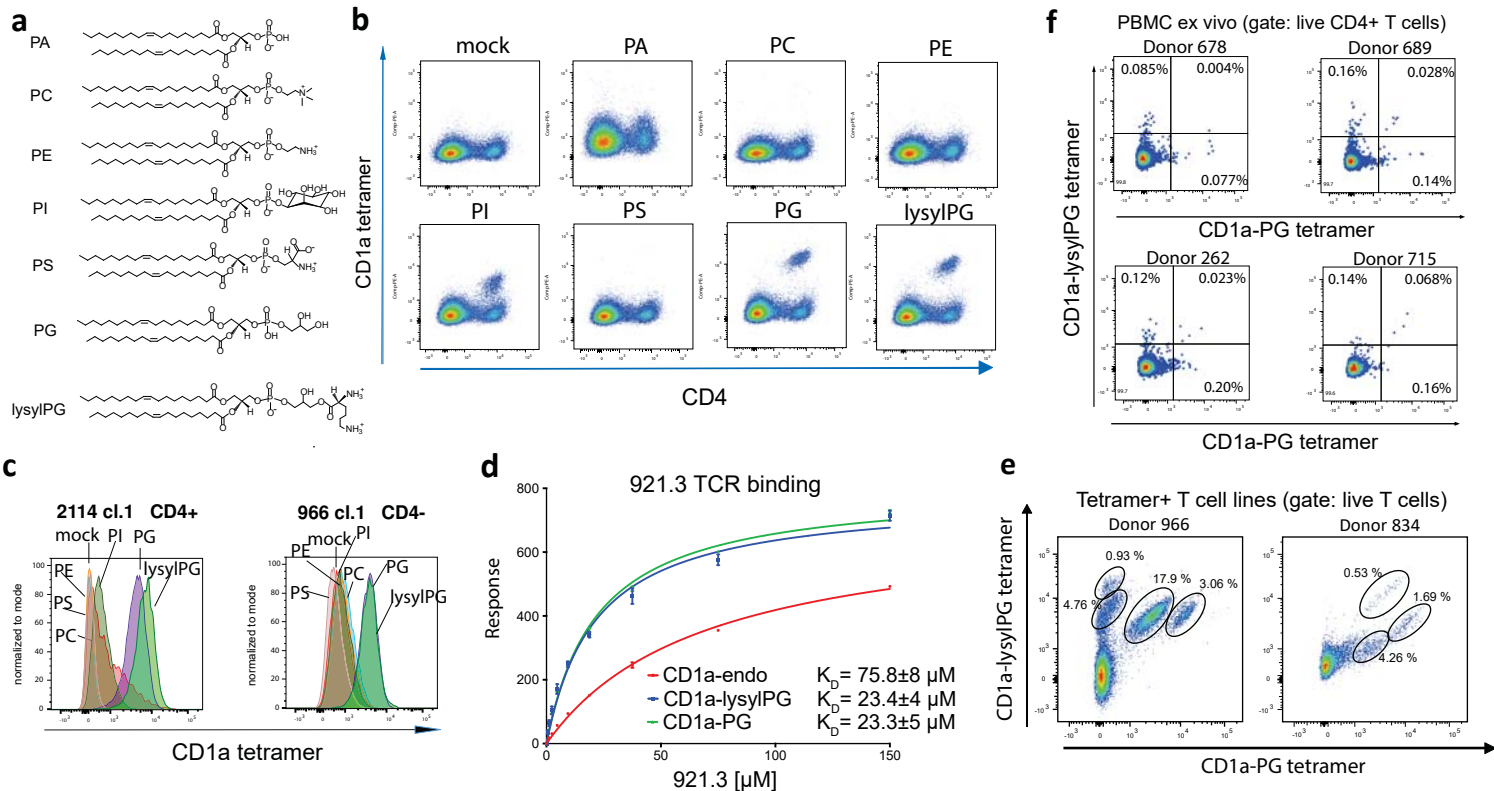
863
864 50. Winn, M.D. *et al.* Overview of the CCP4 suite and current developments. *Acta crystallographica. Section D, Biological crystallography* **67**,
865 235-242 (2011).

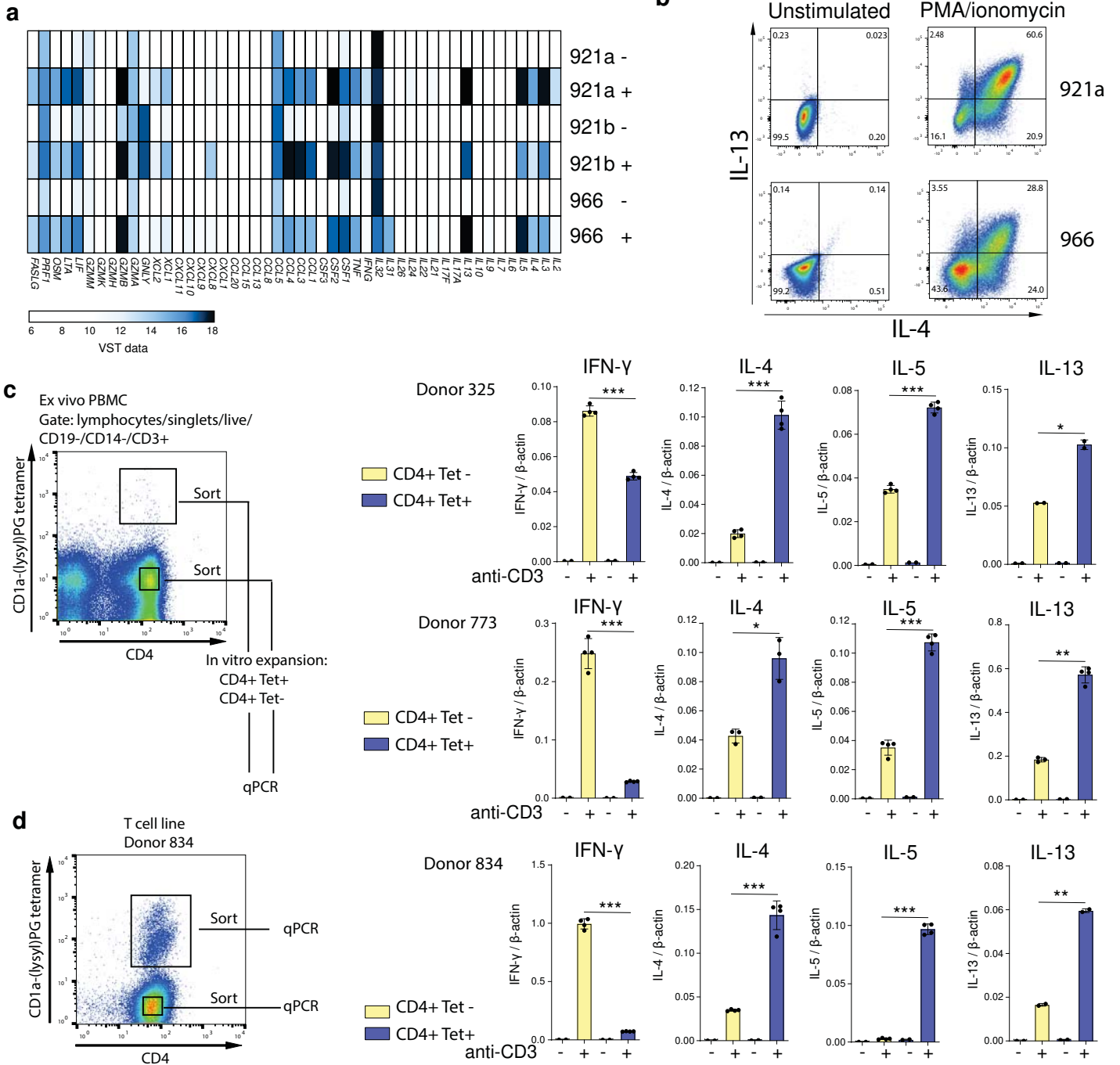
- 866
867 51. McCoy, A.J. *et al.* Phaser crystallographic software. *Journal of applied crystallography* **40**, 658-674 (2007).
- 868
869 52. Emsley, P., Lohkamp, B., Scott, W.G. & Cowtan, K. Features and development of Coot. *Acta crystallographica. Section D, Biological*
870 *crystallography* **66**, 486-501 (2010).
- 871
872 53. Afonine, P.V. *et al.* Towards automated crystallographic structure refinement with phenix.refine. *Acta crystallographica. Section D,*
873 *Biological crystallography* **68**, 352-367 (2012).
- 874
875 54. Bligh, E.G. & Dyer, W.J. A rapid method of total lipid extraction and purification. *Canadian journal of biochemistry and physiology* **37**,
876 911-917 (1959).
- 877
878 55. van 't Klooster, J.S. *et al.* Periprotein lipidomes of *Saccharomyces cerevisiae* provide a flexible environment for conformational changes
879 of membrane proteins. *eLife* **9** (2020).
- 880
881 56. Bush, E.C. *et al.* PLATE-Seq for genome-wide regulatory network analysis of high-throughput screens. *Nature communications* **8**, 105
882 (2017).
- 883
884 57. Lun, A.T.L. & Marioni, J.C. Overcoming confounding plate effects in differential expression analyses of single-cell RNA-seq data.
885 *Biostatistics* **18**, 451-464 (2017).
- 886
887 58. Snyder, M.E. *et al.* Generation and persistence of human tissue-resident memory T cells in lung transplantation. *Science immunology* **4**
888 (2019).
- 889
890 59. Granot, T. *et al.* Dendritic Cells Display Subset and Tissue-Specific Maturation Dynamics over Human Life. *Immunity* **46**, 504-515 (2017).
- 891
892 60. Dobin, A. *et al.* STAR: ultrafast universal RNA-seq aligner. *Bioinformatics* **29**, 15-21 (2013).
- 893

- 894 61. Liao, Y., Smyth, G.K. & Shi, W. featureCounts: an efficient general purpose program for assigning sequence reads to genomic features.
895 *Bioinformatics* **30**, 923-930 (2014).
- 896
897 62. Osorio, D. & Cai, J.J. Systematic determination of the mitochondrial proportion in human and mice tissues for single-cell RNA-sequencing
898 data quality control. *Bioinformatics* **37**, 963-967 (2021).
- 899
900

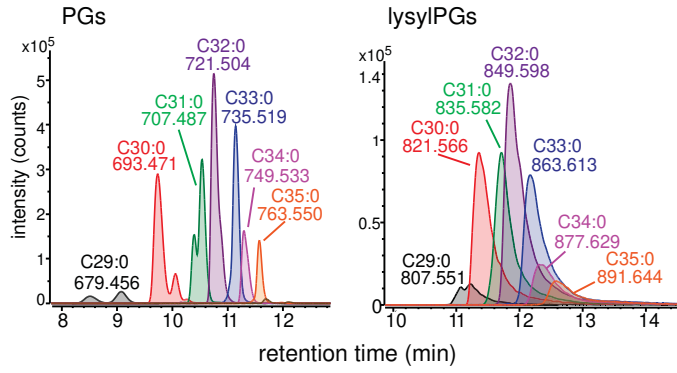




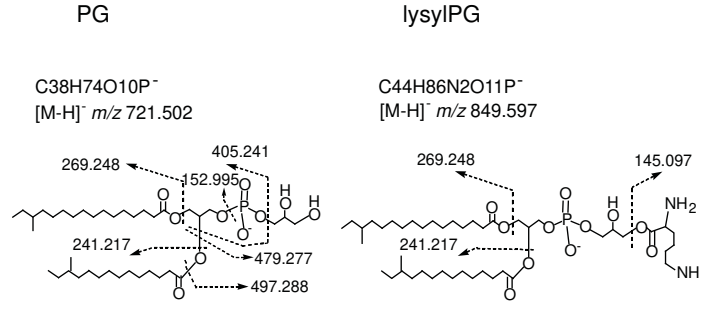




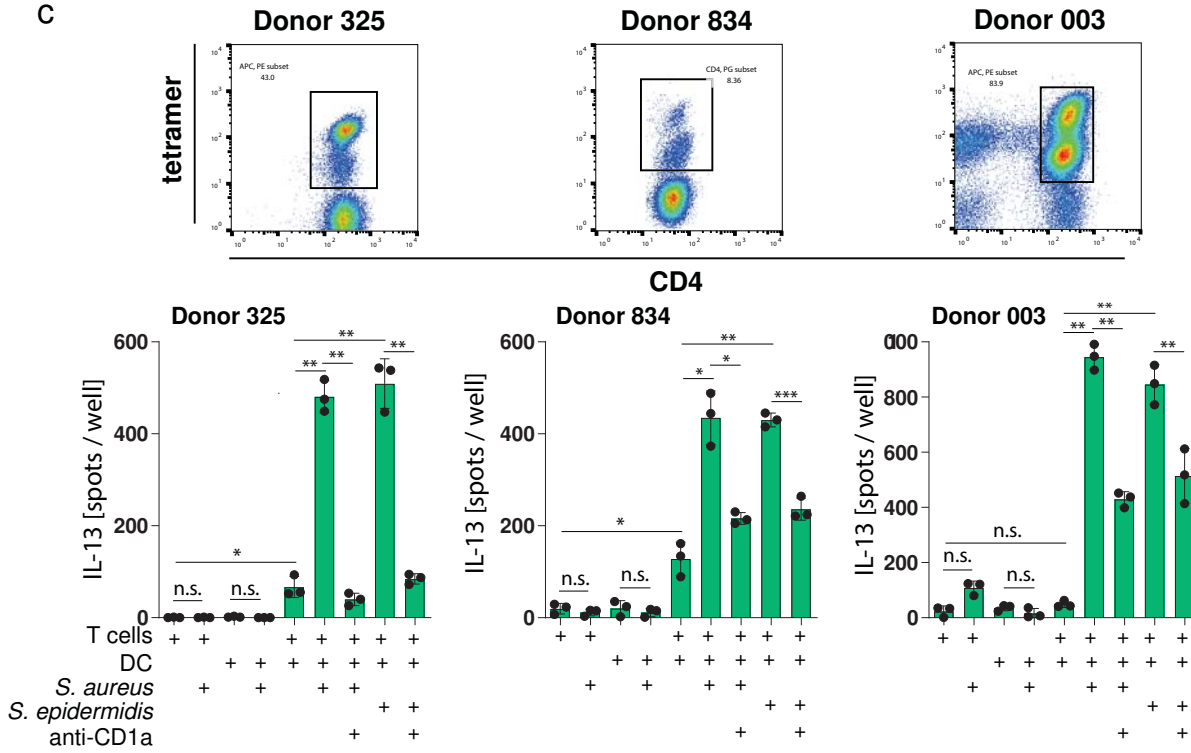
a *S. aureus*



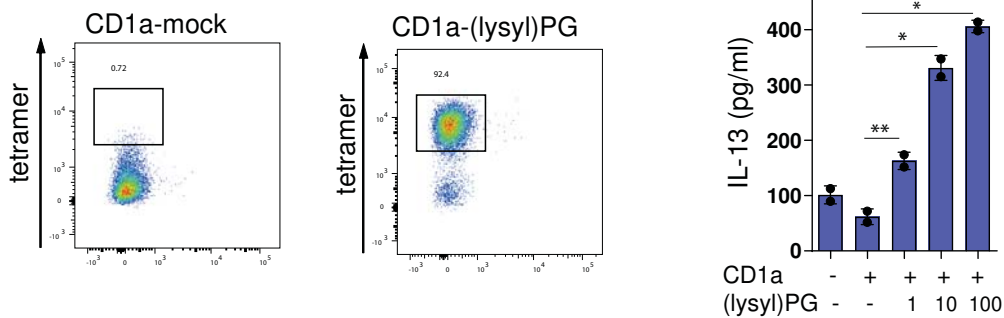
b



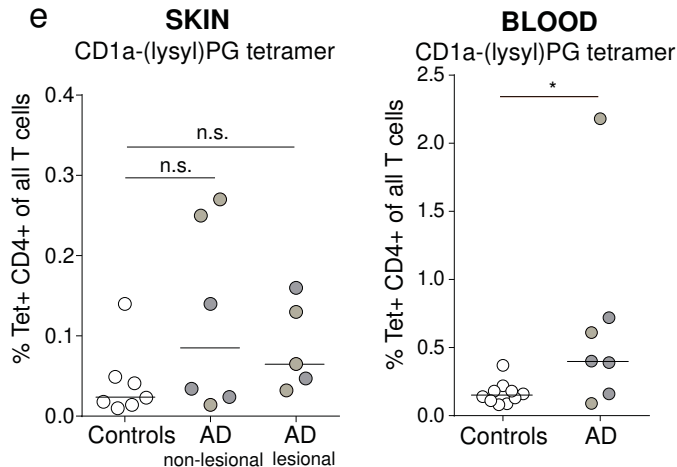
c



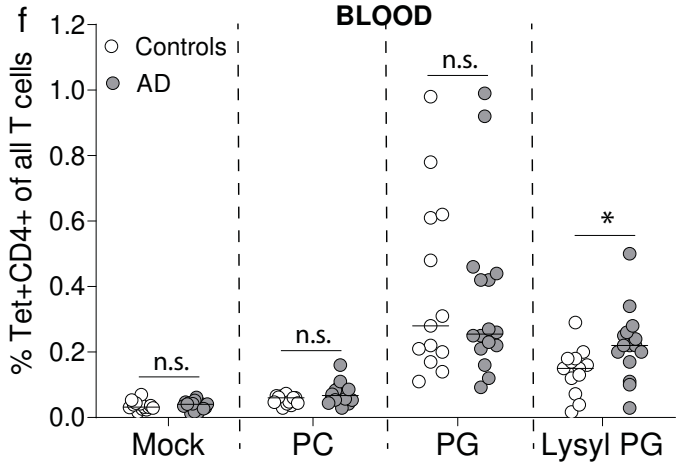
d

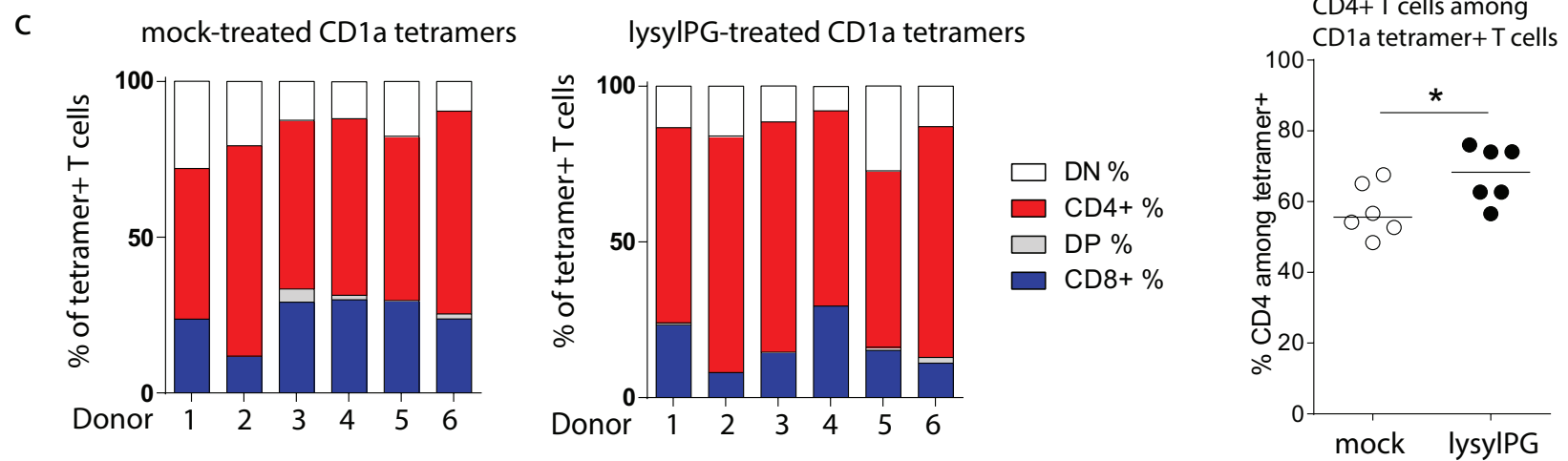
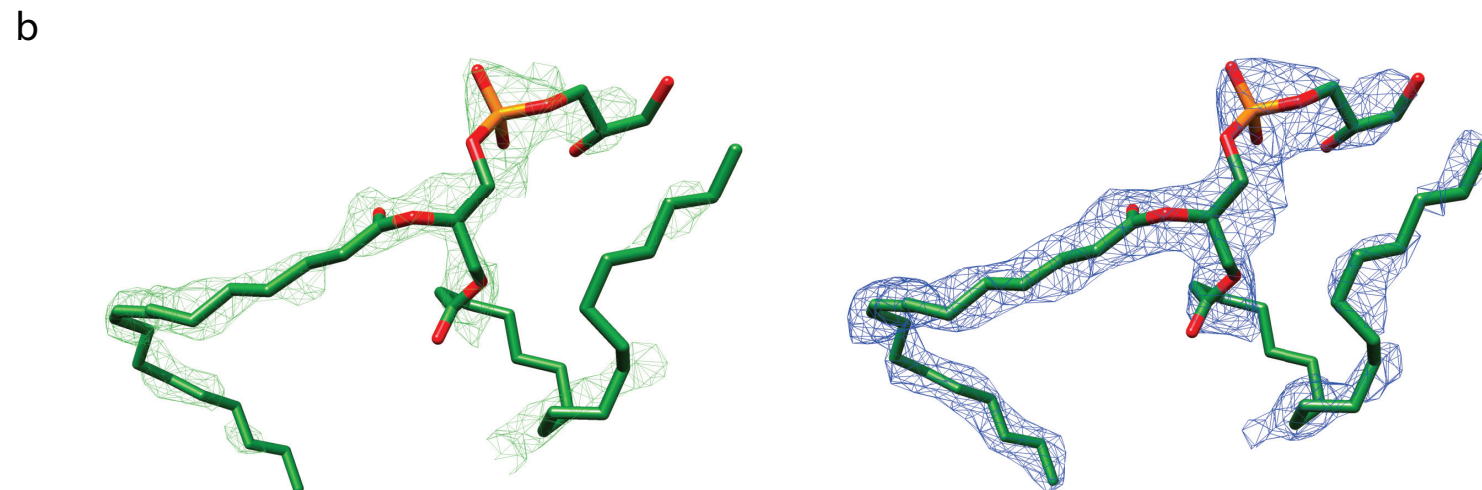
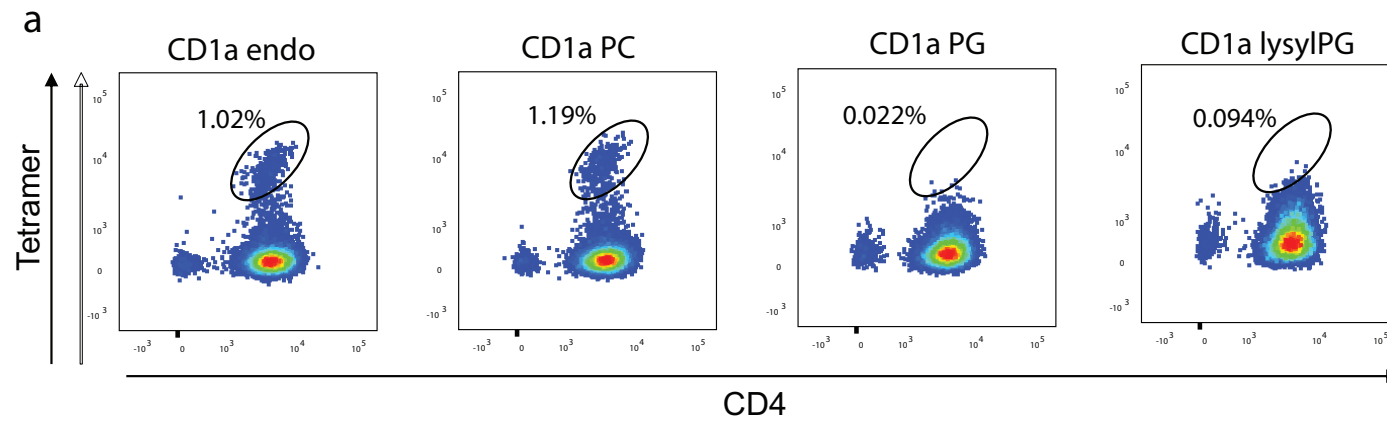


e

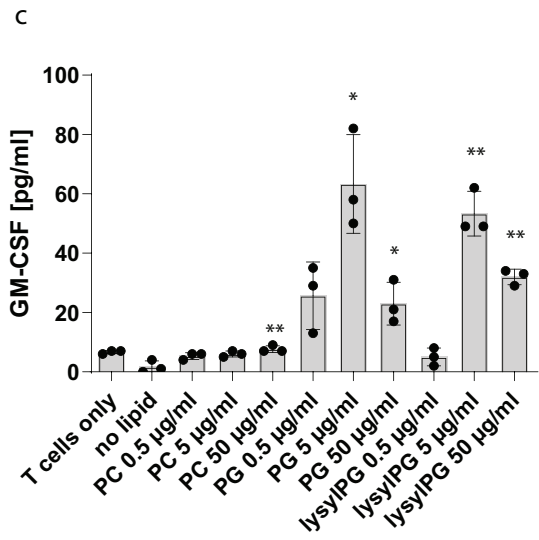
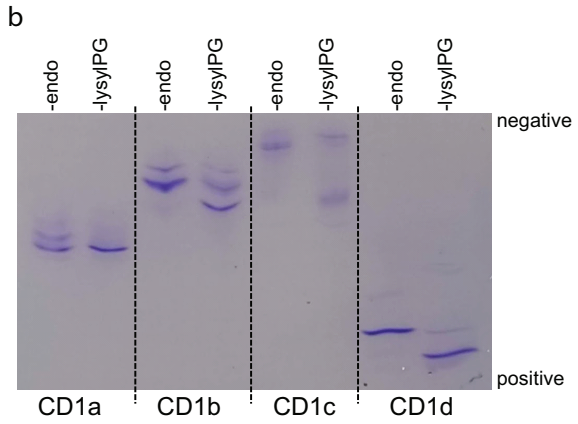
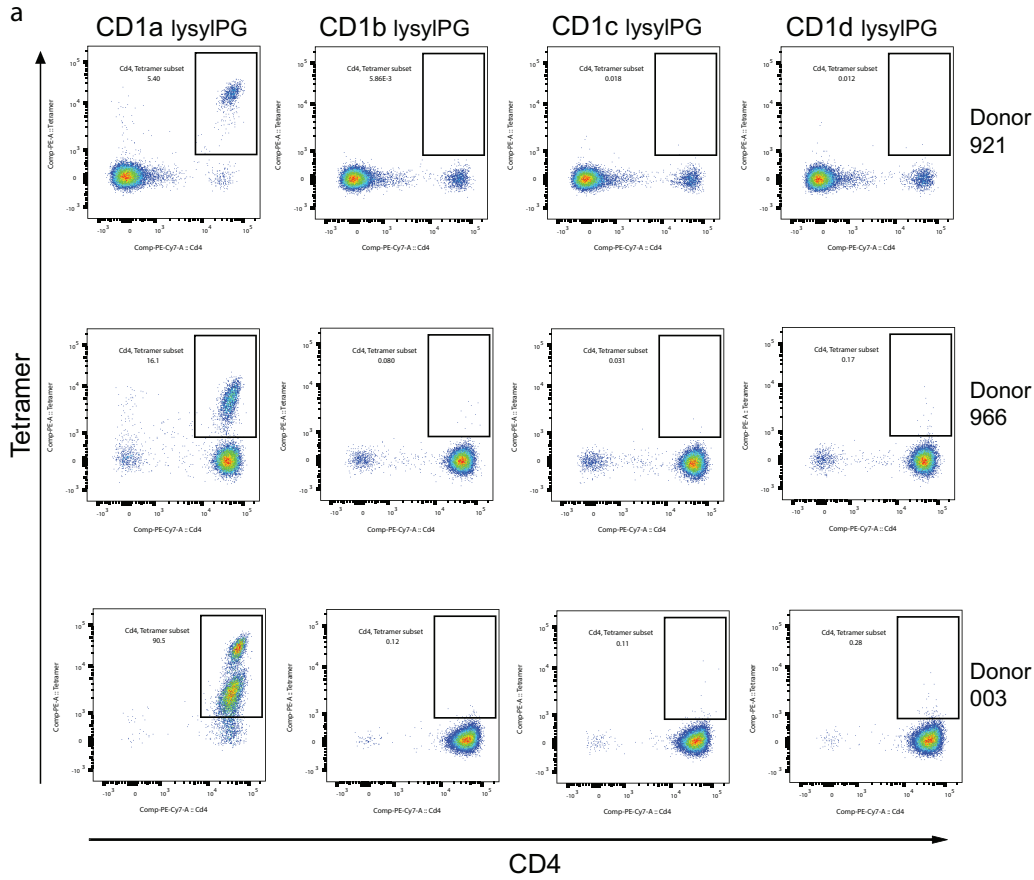


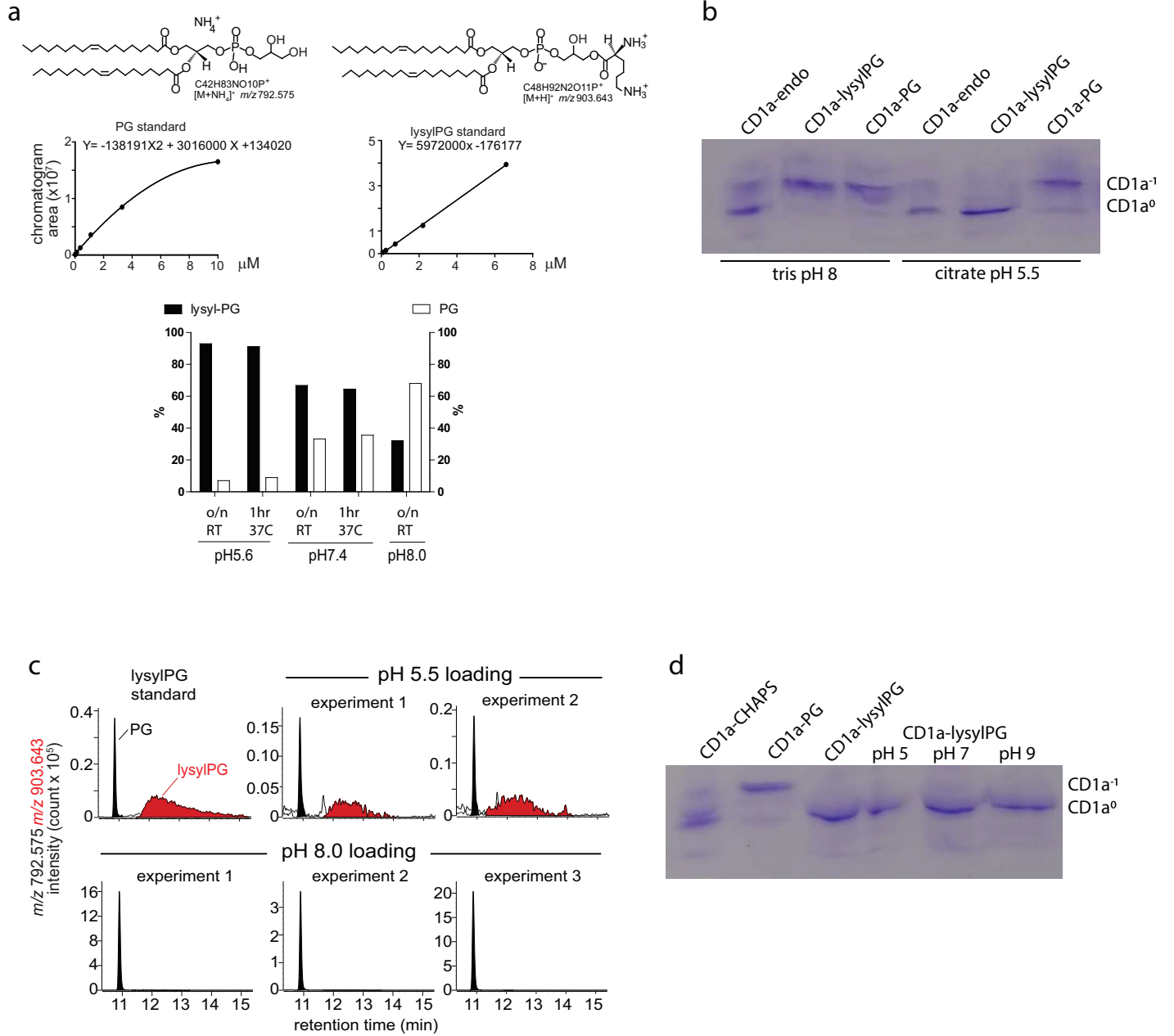
f



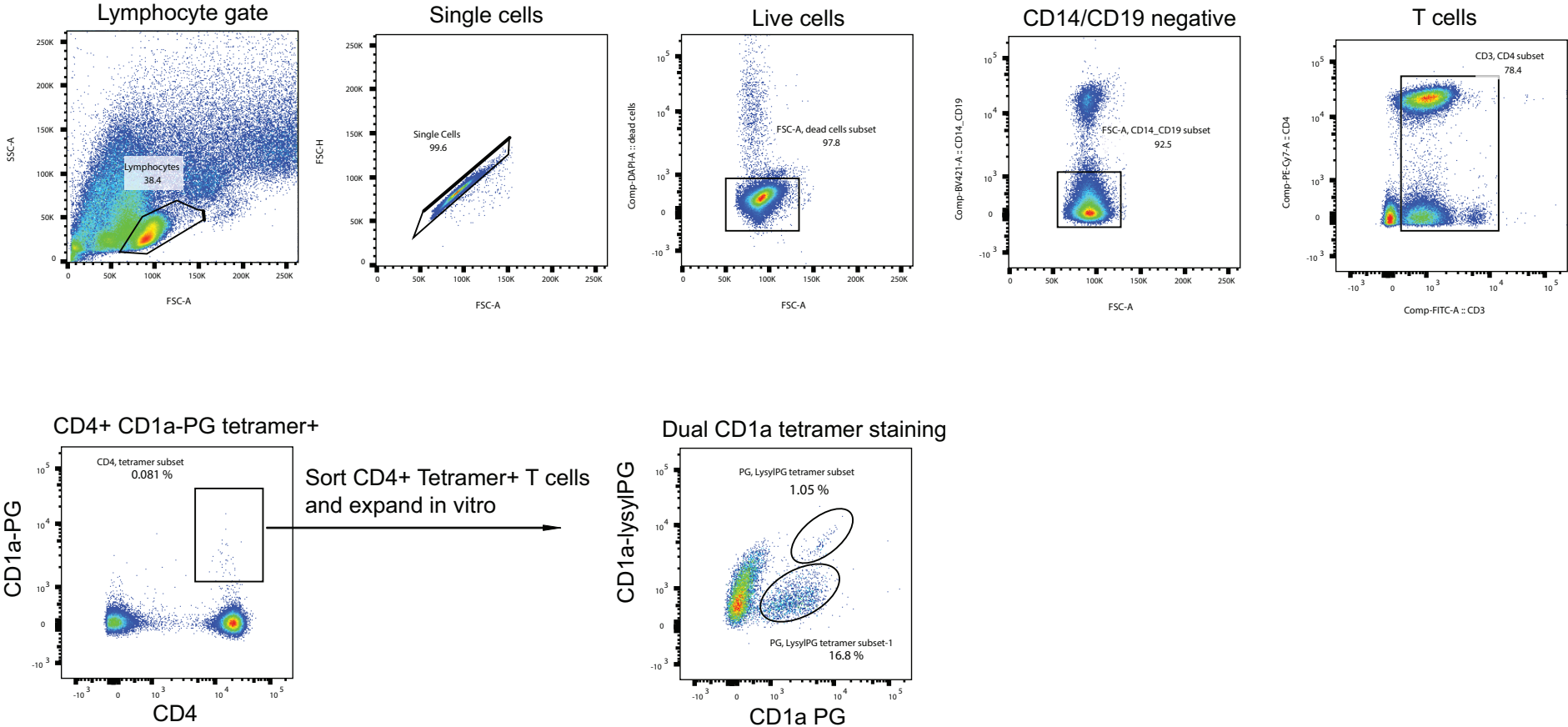


Monnot et al. Extended Figure 2

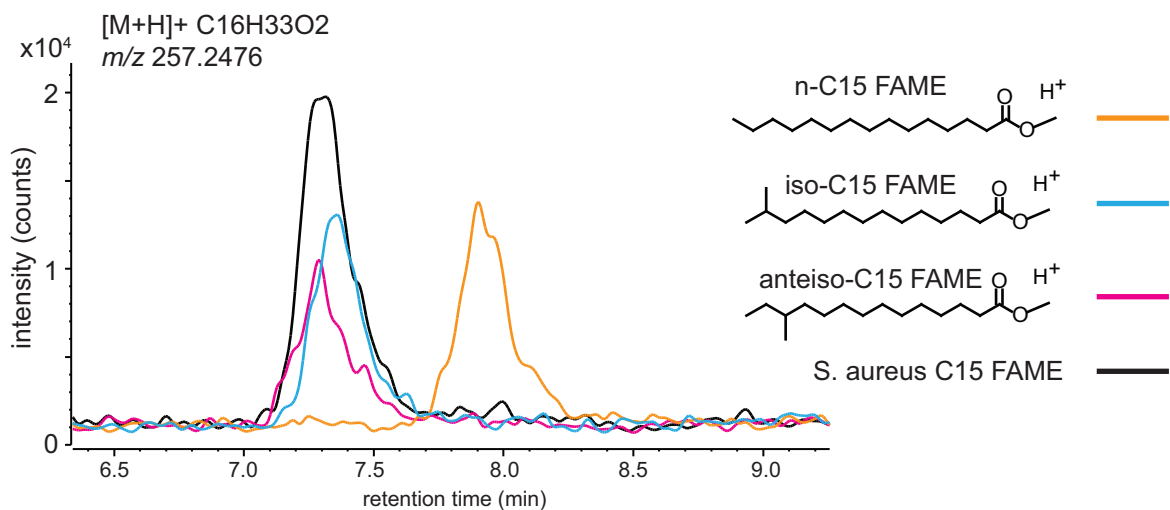




Monnot et al., Extended Figure 4

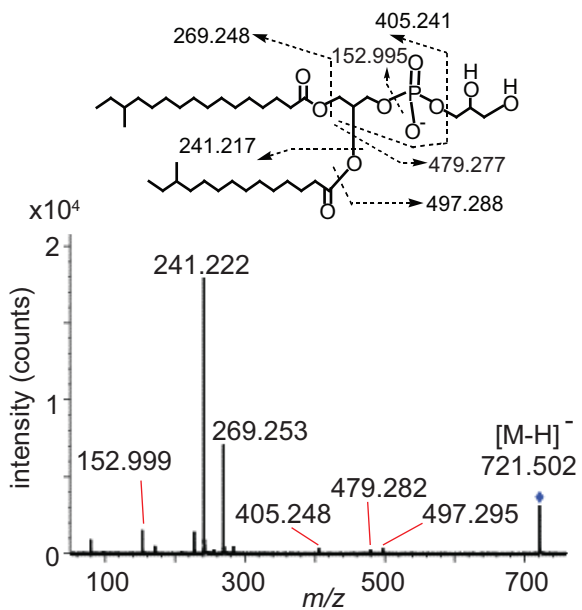


a C15 fatty acid methyl esters



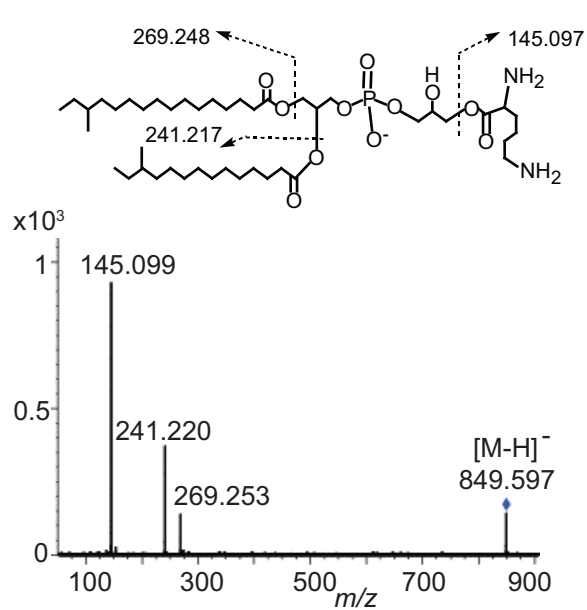
b phosphatidylglycerol

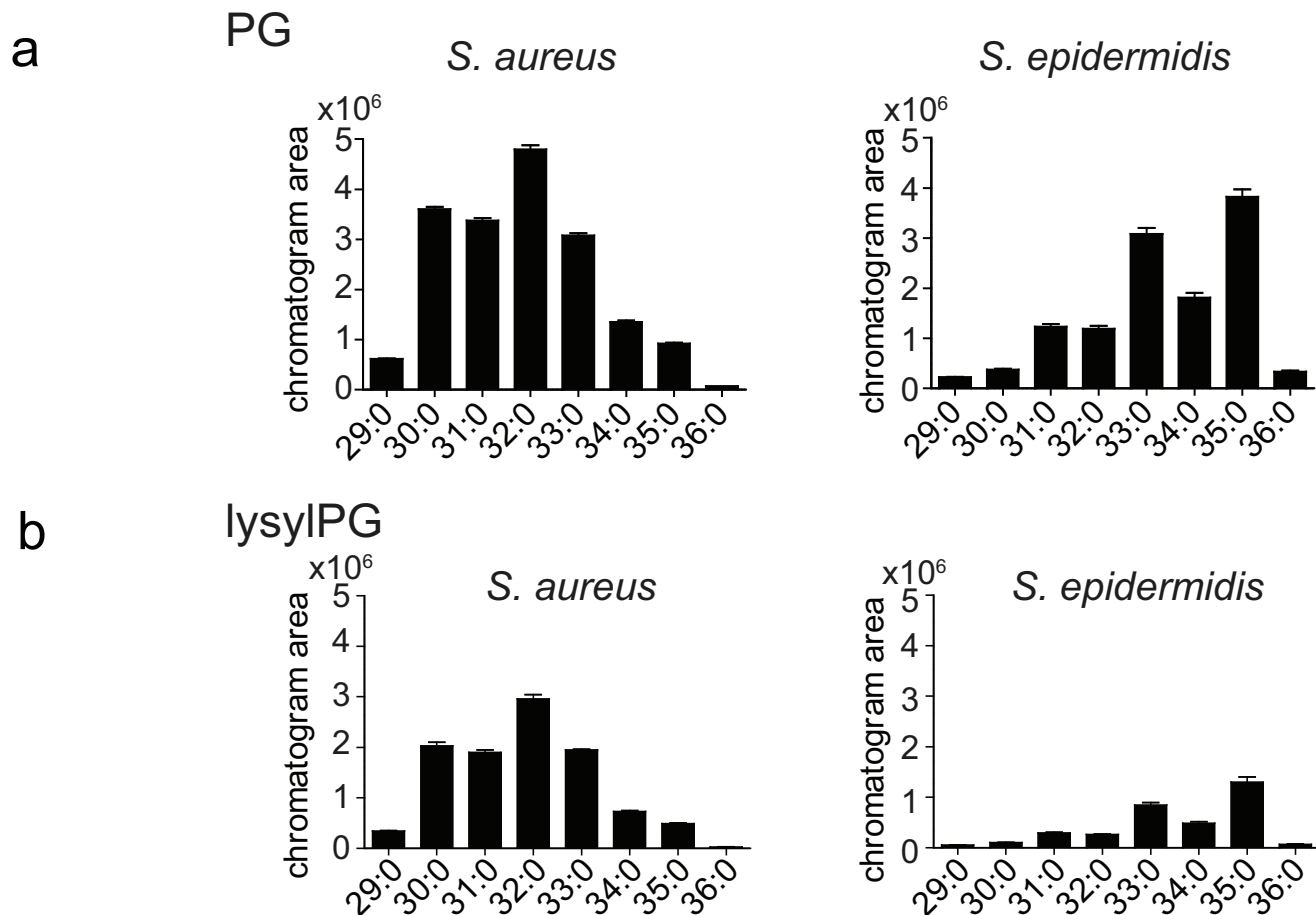
C₃₈H₇₄O₁₀P⁻
[M-H]⁻ m/z 721.502



lysyl phosphatidylglycerol

C₄₄H₈₆N₂O₁₁P⁻
[M-H]⁻ m/z 849.597

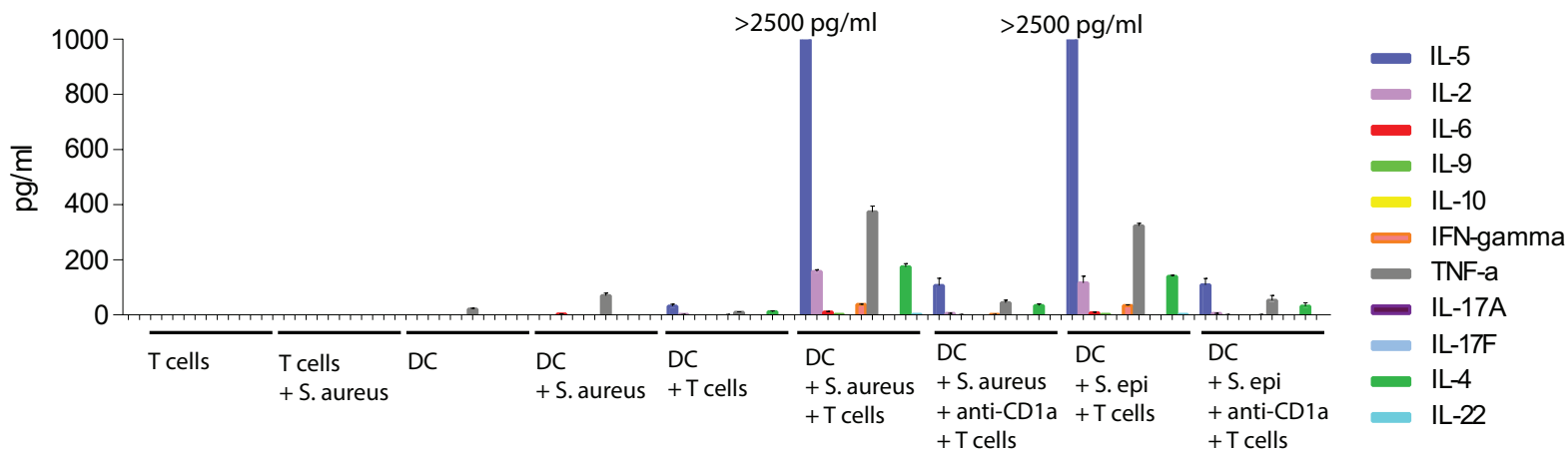




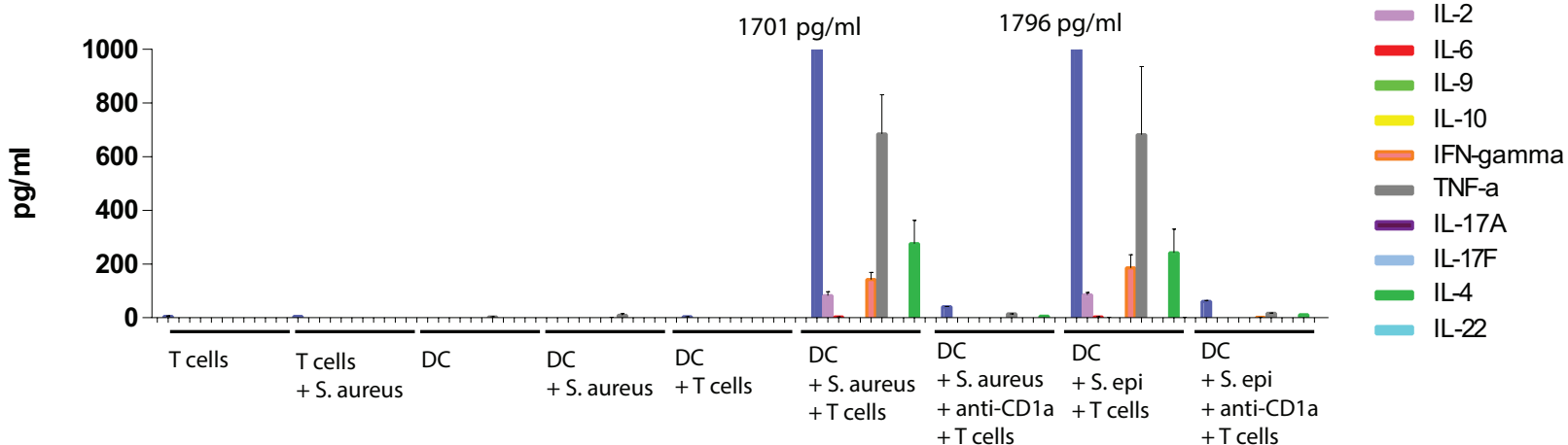
c

detected m/z /lipid chain PG	formula [M-H]-	calculated m/z	estimated amount (ng) in chloroform/methanol extracts (5 µg)	
			<i>S. aureus</i>	<i>S. epidermidis</i>
679.4588/C29:0	C35H68O10P-	679.4556	4.0±0.1	1.1±0.04
693.4755/C30:0	C36H70O10P-	693.4712	33.2±0.6	2.3±0.1
707.4908/C31:1	C37H72O10P-	707.4869	31.0±0.6	9.3±0.5
721.5064/C32:0	C38H74O10P-	721.5025	55.3±2.2	9.1±0.5
735.5223/C33:0	C39H76O10P-	735.5182	28.5±0.6	28.5±1.5
749.5374/C34:0	C40H78O10P-	749.5338	10.9±0.3	15.3±0.9
763.5531/C35:0	C41H80O10P-	763.5495	7.2±0.1	39.8±2.3
777.5674/C36:0	C42H82O10P-	777.5651	0.4±0.002	2.2±0.2
			SUM 170.5±4.1	SUM 107.5±6.0
lysylPG				
807.5521/C29:0	C41H80N2O11P-	807.5505	3.4±0.08	0.8±0.02
821.5684/C30:0	C42H82N2O11P-	821.5662	26.1±1.0	1.5±0.1
835.5837/C31:0	C43H84N2O11P-	835.5818	24.7±0.7	2.9±0.2
849.5993/C32:0	C44H86N2O11P-	849.5975	40.7±1.2	2.5±0.1
863.6147/C33:0	C45H88N2O11P-	863.6131	26.2±0.2	10.5±0.7
877.6296/C34:0	C46H90N2O11P-	877.6288	9.1±0.3	5.7±0.4
891.6449/C35:0	C47H92N2O11P-	891.6444	5.8±0.2	17.5±1.4
905.6586/C36:0	C48H94N2O11P-	905.6601	0.5±0.002	1.1±0.1
			SUM 136.5±3.1	SUM 42.4±3.0

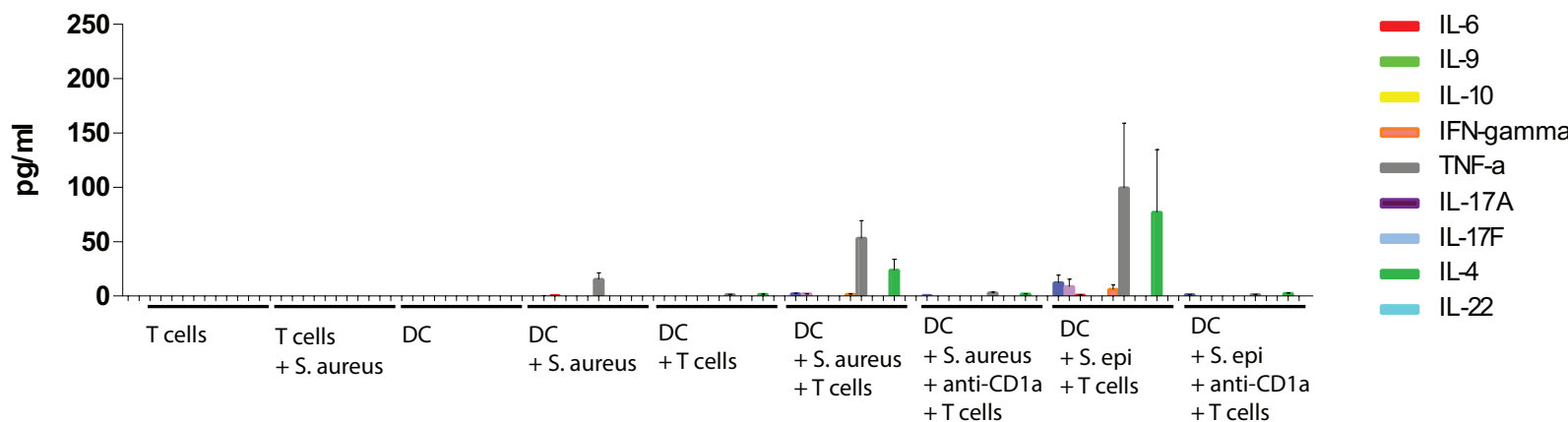
834

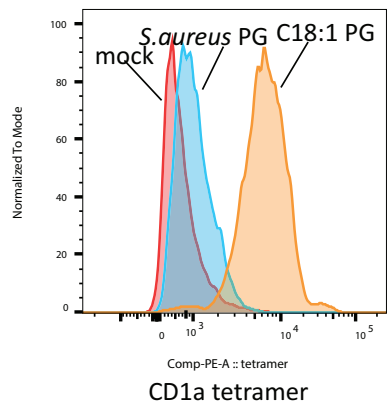
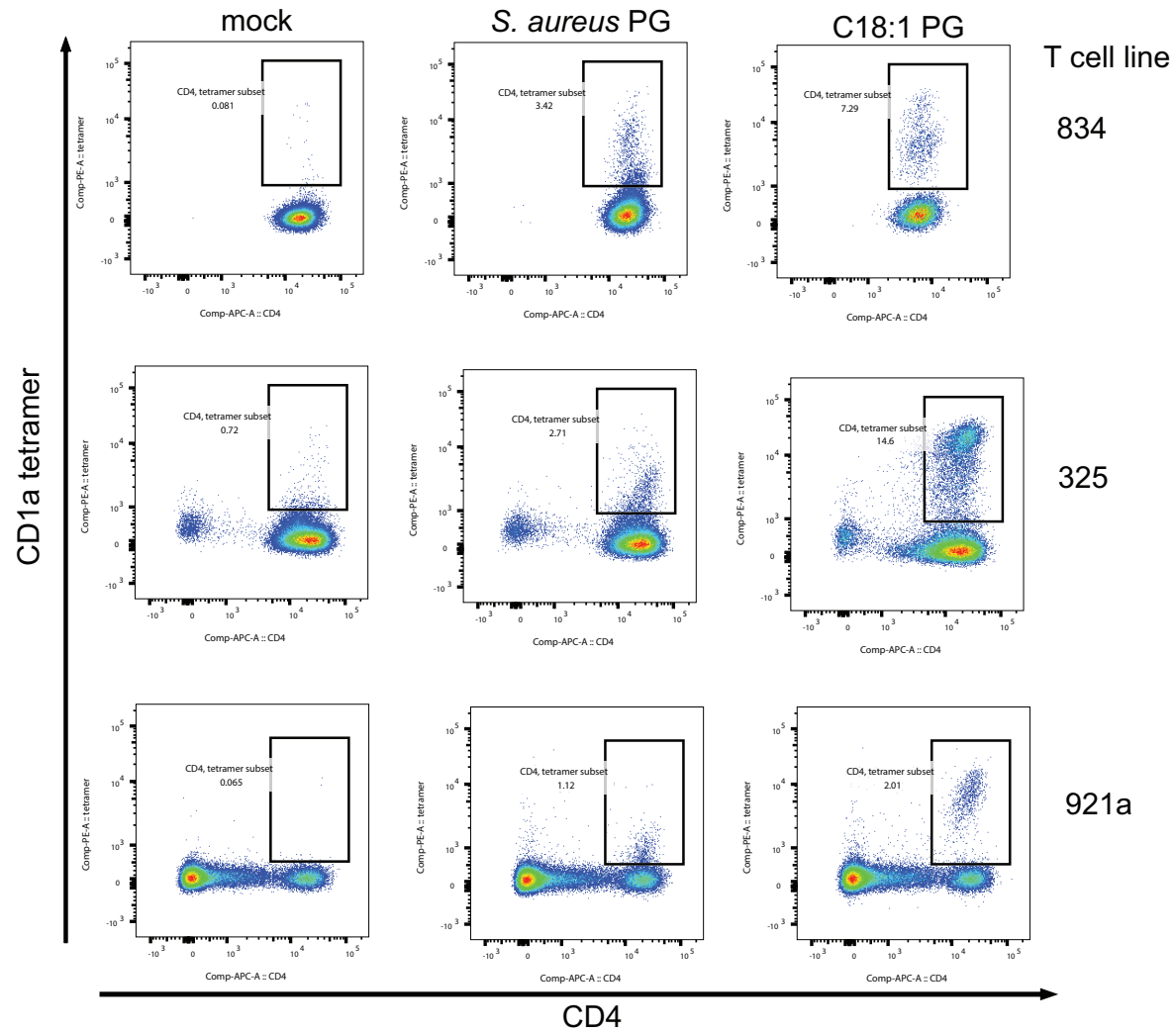


ADE003



325





T cell clone:
2114 cl.1